Physiological and Transcriptomic Evidence for a Close Coupling between Chloroplast Ontogeny and Cell Cycle Progression in the Pennate Diatom *Seminavis robusta*[1][C][W][OA]

Jeroen Gillard, Valerie Devos, Marie J.J. Huysman, Lieven De Veylder, Sofie D'Hondt, Cindy Martens, Pieter Vanormelingen, Katrijn Vannerum, Koen Sabbe, Victor A. Chepurnov[2], Dirk Inzé*, Marnik Vuylsteke, and Wim Vyverman

Laboratory of Protistology and Aquatic Ecology, Department of Biology, Ghent University, B–9000 Gent, Belgium (J.G., V.D., M.J.J.H., S.D., P.V., K.V., K.S., V.A.C., W.V.); and Department of Plant Systems Biology, Flanders Institute for Biotechnology, and Department of Molecular Genetics, Ghent University, B–9052 Gent, Belgium (J.G., V.D., M.J.J.H., L.D.V., C.M., K.V., D.I., M.V.)

Despite the growing interest in diatom genomics, detailed time series of gene expression in relation to key cellular processes are still lacking. Here, we investigated the relationships between the cell cycle and chloroplast development in the pennate diatom *Seminavis robusta*. This diatom possesses two chloroplasts with a well-orchestrated developmental cycle, common to many pennate diatoms. By assessing the effects of induced cell cycle arrest with microscopy and flow cytometry, we found that division and reorganization of the chloroplasts are initiated only after S-phase progression. Next, we quantified the expression of the *S. robusta* FtsZ homolog to address the division status of chloroplasts during synchronized growth and monitored microscopically their dynamics in relation to nuclear division and silicon deposition. We show that chloroplasts divide and relocate during the S/G2 phase, after which a girdle band is deposited to accommodate cell growth. Synchronized cultures of two genotypes were subsequently used for a cDNA-amplified fragment length polymorphism-based genome-wide transcript profiling, in which 917 reproducibly modulated transcripts were identified. We observed that genes involved in pigment biosynthesis and coding for light-harvesting proteins were up-regulated during G2/M phase and cell separation. Light and cell cycle progression were both found to affect fucoxanthin-chlorophyll *a/c*-binding protein expression and accumulation of fucoxanthin cell content. Because chloroplasts elongate at the stage of cytokinesis, cell cycle-modulated photosynthetic gene expression and synthesis of pigments in concert with cell division might balance chloroplast growth, which confirms that chloroplast biogenesis in *S. robusta* is tightly regulated.

Diatoms, an extraordinarily diverse group of heterokontophyte microalgae (Kooistra et al., 2003), dominate the primary production of many marine and freshwater ecosystems (Granum et al., 2005). Based on the shape and structure of their unique siliceous cell walls, two major architectural types are recognized: "centric" diatoms, a paraphyletic group with radially patterned valves, and "pennate" diatoms, a monophyletic group characterized by a feather-like valve structure. Whole-genome sequencing of *Thalassiosira pseudonana* (Armbrust et al., 2004) and *Phaeodactylum tricornutum* (Bowler et al., 2008), representatives of centric and pennate diatoms, respectively, has revealed that they combine plant- and animal-like characteristics and possess many genes that are completely unknown in other organisms. These genome studies enable the unraveling of the genetic basis of the unique properties underlying the ecological and evolutionary success of diatoms. Diatoms have long been known for their extremely high photosynthetic efficiency: compared with other photosynthetic eukaryotic unicells of comparable size, diatoms have the highest growth rates (Banse, 1982; Raven and Geider, 1988; Sarthou et al., 2005) and an unusually high photosynthetic flexibility that is essential for coping with large habitat-intrinsic fluctuations in irradiance (Lavaud et al.,

2004). Their high growth rates might be attributed to their high Rubisco carboxylase efficiency and the putative presence of an alternative C4-photosynthetic pathway, enabling temporary storage of carbon for use at times of low light irradiance (Riebesell, 2000; Wilhelm et al., 2006; Roberts et al., 2007). The photosynthetic flexibility of diatoms is related to their high capacity for energy dissipation through nonphotochemical quenching, which can reach a 5-fold higher level than that in plants (Ruban et al., 2004).

As in other groups of heterokontophyte algae, diatom chloroplasts originate from a secondary endosymbiosis, probably the engulfment of a red alga by a heterotrophic eukaryote (McFadden, 2001; Falkowski et al., 2004). As a result, diatom plastids are surrounded by four membranes instead of the usual two, typical for plants and green algae. Moreover, the outermost pair of membranes is connected with the nuclear envelope in a number of diatoms (Stoermer et al., 1965; Dawson, 1973; Hashimoto, 2005). These characteristics have implications for chloroplast protein targeting pathways (Apt et al., 2002; Kilian and Kroth, 2005) and possibly for its division mechanism and transmission to daughter cells (Hashimoto, 2005). While the chloroplast ultrastructure appears to be fairly uniform in diatoms, there is a wide variation in chloroplast morphology as well as in the number of chloroplasts and their arrangement within the cells. The chloroplasts of polyplastidic diatoms, which comprise most centric diatoms but also several genera of pennate diatoms, have a very simple morphology (for review, see Mann, 1996). In contrast, chloroplasts of mono-, di-, and tetraplastidic diatoms often have more elaborate shapes and can undergo complex changes in morphology and arrangement before and/or after cytokinesis. Chloroplast division involves constriction of the parent chloroplasts into two more or less equally sized daughter chloroplasts. Two types of chloroplast division are recognized among diatoms, referred to as autonomous and imposed division (Mann, 1996). In the autonomous type, believed to be the primitive condition, the chloroplast constricts into two without the obvious involvement of any other organelle. In imposed division, which appears to have evolved several times in different lineages of pennate diatoms, chloroplast division occurs synchronically with the formation of the cleavage furrow. In plants and some other eukaryotes, chloroplast division is orchestrated by a prokaryote-derived division machinery, whose regulation is not fully understood (Osteryoung and Nunnari, 2003; Margolin, 2005; Adams et al., 2008) but should somehow be coordinated with the regulation of the cell cycle machinery that paces the cell division rate on the surrounding environments and coordinates critical processes such as cell growth, karyokinesis, and cytokinesis (De Veylder et al., 2007).

Environmental factors mostly impinge on cell cycle control through cell cycle checkpoints at the G1/S or G2/M cell cycle phase transitions. Many universal core cell cycle genes that regulate these transitions

have been found in the two sequenced diatom genomes (Armbrust et al., 2004; Bowler et al., 2008), but diatom-specific genes and gene regulations may contribute to the unique features that distinguish diatoms from other algae (Montsant et al., 2007; M.J.J. Huysman, A. De Martino, C. Martens, E. Rayko, J. Gillard, M. Heijde, B. Mathieu, A. Meichenin, A. Montsant, K. Vandepoele, Y. Van de Peer, L. De Veylder, D. Inzé, C. Bowler, and W. Vyverman, unpublished data). Chloroplast development is difficult to address in polyplastidic cells, such as centric diatoms and cells of higher plants (Pyke, 1999). However, the observed coordination of chloroplast development with cell cycle progression in many pennate diatoms creates an opportunity to address more easily chloroplast development in relation to other cellular processes, because if chloroplast ontogeny is regulated by the cell cycle, the controlled progression of chloroplasts can be studied in synchronized cultures.

Here, we combined physiological experiments, cytological observations, and a cDNA-amplified fragment length polymorphism (AFLP)-based genome-wide transcriptome analysis to identify cell cycle-dependent checkpoints in chloroplast development and gene expression during synchronized growth. As a model species, we used *Seminavis robusta* (Danielidis and Mann, 2002), a representative of the diverse and ecologically important group of pennate Naviculaceae. As in most genera of this family, the two chloroplasts in *S. robusta* divide in an autonomous manner and move from the girdle to the valves and back, once during each cell cycle (Chepurnov et al., 2002; Supplemental Fig. S1). *S. robusta* is particularly well suited for cytological studies because of its large size (up to 100 μm) and, being a benthic species adhering to surfaces (Thompson et al., 2008), the easy and nonintrusive observation of cellular behavior. Moreover, sexual reproduction can be controlled, resulting in the first diatom pedigree that currently comprises approximately 110 clones (Chepurnov et al., 2008). Therefore, this species offers interesting perspectives for functional genomics studies as well as for forward genetics to investigate key life history traits, including the dynamics of their photosynthetic apparatus and its interaction with other cellular processes and the environment.

RESULTS

Cell and Chloroplast Division Are Both Arrested in Response to Darkness and Cell Cycle Inhibitor Treatments

Using light deprivation and two cell cycle inhibitors, we investigated whether a relationship exists between the cell cycle checkpoints and the chloroplast division cycle. For light deprivation, exponentially growing cultures were transferred to complete darkness for 24 h and compared with light-grown control cultures by

flow cytometry (Fig. 1A). The tetraploid peak (G2+M phase) present in the light-grown cultures was absent in the 24-h dark-treated cultures, indicating that in the latter the majority of cells were arrested in the G1 phase of the cell cycle. Microscopically, the light-grown cultures consisted of both dividing and nondividing cells (Fig. 1B). In contrast, the dark-arrested cultures only contained nondividing cells (Fig. 1C). These cells have their two chloroplasts undivided and located at the girdle sides of the cell (Fig. 1, D–G). In most cases, the ventral chloroplast had four subcentral lobes that, across the valves, reached the dorsal side of the cell (Fig. 1, F and G). Occasionally, some postcytokinetic doublet cells could also be found in the dark-arrested cultures. These doublet cells are at a stage after cytokinesis but before cell separation, during which the cell is devoted to frustule formation (Coombs et al., 1967a). Microscopically, the doublet cells in dark-arrested cultures contained the G1 type of girdle-located undivided chloroplasts.

Next, we studied chloroplast behavior upon treatment with chemical cell cycle inhibitors. First, hydroxyurea (HU) was applied to exponentially growing c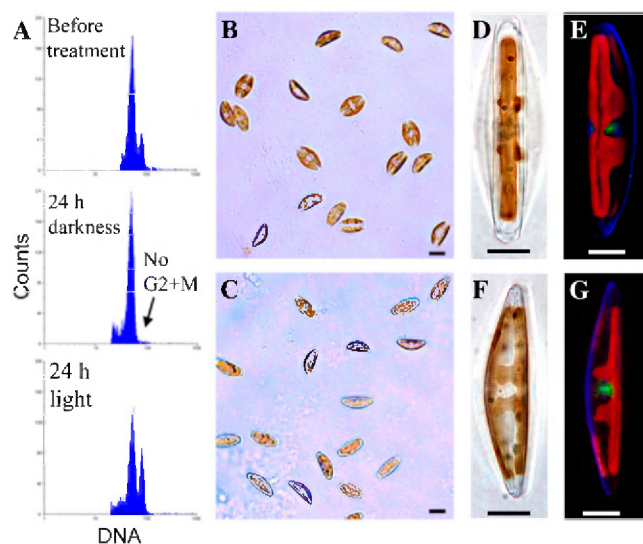ultures, thereby inhibiting S-phase progression by depleting the cell of deoxynucleoside triphosphates (Young and Hodas, 1964). A complete S-phase arrest of cell division by HU was confirmed by flow cytometry after 72 h of treatment (Supplemental Fig. S2), while the cultures remained healthy, because cell growth restarted after the inhibitor had been washed away (data not shown). The cells in these S-phase-arrested cultures all contained girdle-located undivided chloroplasts as in dark-arrested G1-phase cells, but the subcentral lobes were not observed (Fig. 2A). From these observations, we conclude that chloroplast division and movements do not take place before the S phase. However, these results should be interpreted with caution: because HU depletes the cell's deoxynucleoside triphosphate pool, chloroplast DNA replication might be affected by the drug and, thus, inhibition of plastokinesis might be a direct effect of the chloroplast's inability to replicate its DNA. To validate these findings, aphidicolin, another cell cycle S-phase inhibitor that blocks the nucleus-specific DNA polymerase α (Ikegami et al., 1978), was applied on dark-arrested cultures that were reilluminated immediately after addition of the drug. Microscopic analysis after 24 h revealed that treated cells did not divide and contained undivided chloroplasts located at the girdle sides (Fig. 2, B–D), while control cultures divided normally. In contrast with HU-arrested cells, ventral chloroplast lobes were observed during aphidicolin arrest (Fig. 2D).

Cytological Changes during Cell Cycle Progression in Synchronized Cultures

Based on the uniform cell cycle arrest in dark-arrested cultures, we established a synchronization procedure to study cell cycle-modulated processes. To this end, exponentially growing cultures (12 h:12 h light:dark) were transferred into darkness for a period of 24 h and reilluminated for 12 h. Two monoclonal strains, designated F_1-8B and F_1-9A, were synchronized in this manner and were used for the transcriptome analysis described below. Reillumination resulted in the synchronous reactivation of cell cycle progression, starting from the G1 phase of the dark-arrested cells. Synchrony was evaluated by estimating the amount of dividing cells at hourly intervals, complemented by observations of chloroplast dynamics (Fig. 3). Dividing cells were operationally defined to include only doublet cells, characterized by the presence of a cleavage furrow, which is visible as an area of high contrast separating the chloroplast pairs (see Supplemental Fig. S3 for an illustration of the counting procedure). Immediately upon reillumination, all cells were in the G1 phase, containing undivided chloroplasts as previously shown. After 4 h, few cells with divided chloroplasts appeared in the cultures, and after 6 h, some cells were dividing. From 6 h onward, the cultures contained S-, G2-, and M-phase cells, in which the proportion of dividing cells progressively increased until 50% at the 9-h sampling

Figure 1. Response of *S. robusta* to dark treatments. A, Flow cytometric DNA content histograms of an exponentially growing culture before transfer to darkness (top), after 24 h of dark incubation (middle), and after 24 h of light (bottom). B to D and F, Light microscopic photographs of the 24-h light-treated culture (strain F_1-8B; B), the 24-h dark-treated culture (strain F_1-8B; C), a 24-h dark-arrested cell in girdle view with focus on the ventral chloroplast (strain F_2-31B; D), and a 24-h dark-arrested cell in valve view (strain F_2-31B; F). The chloroplasts appear brownish, and the cell wall is visible due to its high contrast. E and G, Confocal fluorescence microscopic photographs of cells from dark-arrested cultures (strain F_2-31B) in which the chloroplastidic signal is red (autofluorescence), the nuclear signal is green (SYBR Safe), and the cell wall signal is blue (PDMPO; Lysosensor). Chloroplasts of dark-arrested cultures are undivided and pressed against the girdle. The ventral chloroplast has four subcentral lobes that extend across the valve toward the dorsal side of the cell. Bars = 10 μm.
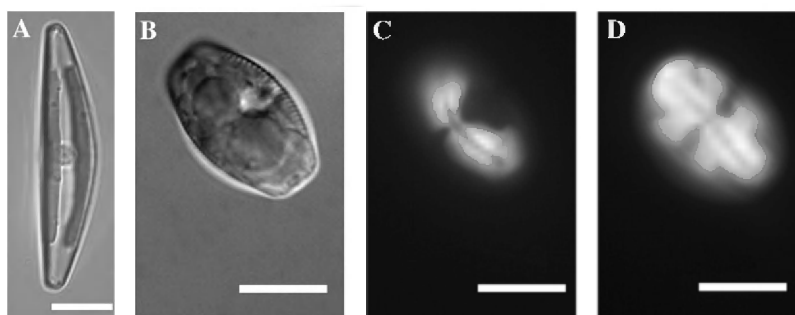
Figure 2. *S. robusta* cells in cell cycle inhibitor-treated cultures. A and B, Light-microscopic photographs. C and D, Fluorescence microscopic photographs. A, HU-treated cell (strain F_2-31B) arrested during S phase. B to D, Aphidicolin-treated cell (strain F_1-8B) in girdle view (B) with focus on the ventral chloroplast (C) and on the dorsal chloroplast (D). In each case, both chloroplasts are undivided and located against the valves. The difference in cell morphology between cells in A and B to D is due to the different average cell sizes of the strains used. Bars = 10 μm.

point. At 9 h, the amount of dividing cells decreased as a consequence of daughter cell separation and initiation of the second cell division cycle.

The phenotypic cell cycle events during synchronization of the cultures were further characterized with confocal laser-scanning microscopy and an appropriate set of stains for the nucleus (SYBR Safe) and the cell wall (2-(4-pyridyl)-5-((4-(2-dimethylaminoethylamino-carbamoyl)methoxy)phenyl)oxazole [PDMPO]). Besides fluorescent cell wall labeling in diatoms (Shimizu et al., 2001; Leblanc and Hutchins, 2005), PDMPO visualizes acidic organelles (Diwu et al., 1999) and monitors the location of newly incorporated silica.

As shown previously by Chepurnov et al. (2002), chloroplast division occurs by central constriction (Fig. 4A), and upon completion of constriction of the dorsal (Fig. 4B) and ventral (Fig. 4C) chloroplasts, the daughter chloroplast pairs move bodily in opposite directions, describing a circular motion along the periphery of the cell, until they position against the valves (Fig. 4, D and E; see also Supplemental Fig. S1). By comparing these cells with the dark-arrested cells in valve and girdle views (compare Fig. 1G with Fig. 4D and Fig. 1E with Fig. 4E), the difference in location between undivided and divided chloroplasts could easily be seen. During this "reorganized chloroplast configuration" stage, the nucleus, positioned in the center of the cytoplasm, was still undivided (Fig. 4E). Taking into consideration that the chloroplasts divide after S-phase initiation, this shows that plastokinesis and subsequent chloroplast relocation occur during S/G2 phase and are fully established before M phase.

Before signs of mitosis appeared, but after chloroplast rearrangement, the first PDMPO signal was detected as an elliptically shaped thin band (Fig. 4F). This signal probably represents a girdle band (Supplemental Fig. S4) that is added to the girdle as a result of cell growth. Chloroplast reorganization was followed by karyokinesis (Fig. 4G) and cytokinesis (Fig. 4, H–K). Early on during cytokinesis, PDMPO fluorescence was initially detected inside two "vacuole-like" compartments located against the division plane

running from pole to pole (Fig. 4H), while a PDMPO-stained cell wall was not yet visible. Since the fluorescence emission and intensity of PDMPO typically shift when the intracompartmental silica concentration increases above 3.2 mM (Shimizu et al., 2001; Hazelaar et al., 2005), the observed fluorescence of PDMPO in these compartments could be paralleled with silicon influx in preparation for silica deposition during the subsequent formation of the frustule. The deposition of cell wall material was observed as a straight line that ran between the two daughter nuclei and located

Figure 3. Evaluation of the synchrony of cell and chloroplast division in *S. robusta* synchronized strains F_1-8B and F_1-9A. The proportion of dividing cells is presented as a function of time, during reillumination of the 24-h dark-arrested cultures. Data are means ± SE of six microscopic fields (0.09 mm²). The predominant morphological stages in each cell cycle phase are represented from light to dark gray in this order: undivided chloroplasts, dividing chloroplasts, dividing cells, and separating cells. G1 corresponds to the phase in which cells with undivided girdle-located chloroplasts are present. The asterisk denotes the first observed cells with divided chloroplasts and also approximates the moment of S-phase initiation, according to the transcriptional induction of the MCM5 prereplication factor (Supplemental Fig. S8). G2/M corresponds to the phase in which dividing cells were increasingly represented with a maximum in the amount of dividing cells at 9 h. M/G1 corresponds to the stage of cell separation.

Figure 4. Cytological events during synchronized growth of *S. robusta* observed by confocal fluorescence microscopy. The chloroplastidic signal is red (autofluorescence), the nuclear signal is green (SYBR Safe), and the silica tracer signal is blue (PDMPO; Lysosensor). In photographs A, C, D, and H, the transmis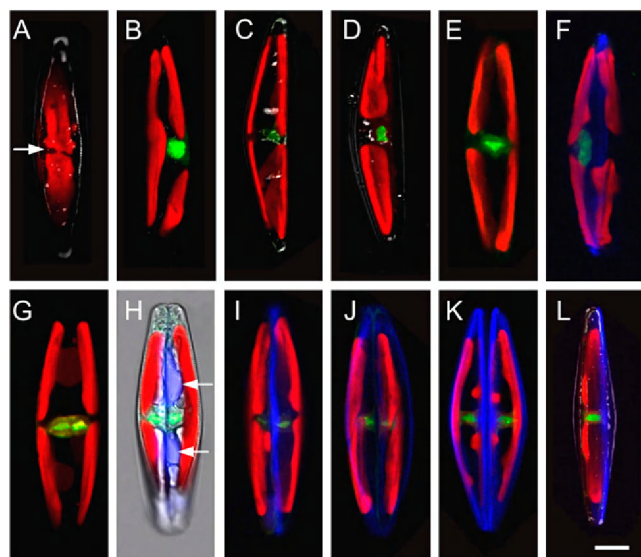sion light channel was permitted in order to visualize the outline of the cell. B to D, Cells shown in valve view. A, E to J, and L, Cells shown in girdle view. A, Cell with focus on a dividing dorsal chloroplast, displaying the central constriction (arrow). B, Cell with the dorsal chloroplast divided. C, Cell with both chloroplasts divided. D and E, Cell with fully rotated, valve-located chloroplasts and containing an undivided nucleus. F, Cell with valve-located chloroplasts and showing a blue band in the middle of the cell, extending from pole to pole. This band probably represents a girdle band (Supplemental Fig. S4). G, Cell just after karyokinesis. Each daughter nucleus is situated on a different side of the future division plane. H, Cell during cytokinesis. The division of the protoplast is apparent by the cleavage furrow, visible as a line of higher contrast running from pole to pole and in between both daughter nuclei. The PDMPO signal is confined to two "vacuole-like" compartments; as such, it appears that deposition of silica at the site of the cleavage furrow has not yet begun. I, Dividing cell during frustule formation. Deposition of silica into the frustule is visible as a line running from pole to pole and situated between the chloroplast pairs and daughter nuclei. J, Dividing cell with chloroplasts moving back from the valves toward the girdle. K, Separating daughter cells in slightly tilt valve view with focus on the dorsal chloroplasts, which are completely covering the girdle area. From the ventral chloroplasts, only the subcentral lobes are visible. L, A newly divided cell with the newly formed valve stained with PDPMO. The other valve is inherited from the mother cell. Bar = 10 μm.

at the site of the previously observed cleavage furrow (Fig. 4I). Only after this initial deposition of silica, while both cells were still attached to each other, the chloroplasts moved back from the valves to the ventral and dorsal girdle sides (Fig. 4J). During this last relocation event, each chloroplast elongated until it completely covered the girdle area. Cell division was finalized when daughter cells separated (Fig. 4K), creating two new cells containing one unstained valve, inherited from its mother, and one newly built valve stained with PDPMO (Fig. 4L).

Cell Cycle-Modulated Expression of the *S. robusta* Chloroplast Division Protein FtsZ

The microscopically derived indications of cell cycle phase-dependent chloroplast division were validated by transcript quantification of the bacterial cell division homolog *FtsZ* in synchronized *S. robusta* cultures. Therefore, a *FtsZ* gene fragment was amplified with a set of nested degenerate primers, cloned, and sequenced, enabling the design of a specific primer pair suited for real-time (RT) quantitative (Q) PCR (Supplemental Fig. S5). Three constitutively expressed genes were used for data normalization (see "Materials and Methods"), and RT-Q-PCR of the *S. robusta FtsZ* ortholog was done on two replicated synchronizations of strain F_1-8B (Fig. 5). Both showed that *FtsZ* expression is modulated during synchronization. Its expression 5 to 8 h after reillumination increased 2.5- to 4-fold when compared with its average expression between 0 to 4 h. In both replicates, *FtsZ* was maximally expressed at 7 h after darkness, being 2 h before most cells were dividing.

cDNA-AFLP Expression Profiling during Cell Cycle Progression

In parallel with the above-described sampling (Fig. 3) for cytological observations, samples were taken at 1-h intervals to conduct a cDNA-AFLP-based genome-wide transcript profiling to identify modulated gene expression profiles correlated with the cytological changes during the cell cycle. The complete data set, including annotations and expression data, is available online (Supplemental Table S1).

The cDNA-AFLP analysis resulted in 2,908 transcript-derived fragments (TDFs) that were scored quantitatively. A considerable amount of expression variation between the two strains originated from genotype-dependent DNA polymorphisms in the transcripts, resulting in the absence/presence of cDNA-AFLP fragments

Figure 5. Expression of the *S. robusta* FtsZ ortholog as a function of time after reillumination during two replicate synchronizations of strain F_1-8B. The proportion of dividing cells is presented as a function of time during reillumination together with the relative expression values of *FtsZ*. RT-PCR data were normalized against three cDNA-AFLP-acquired reference genes. [See online article for color version of this figure.]

(see Supplemental Fig. S6 for an example of a cDNA-AFLP electropherogram; Vuylsteke et al., 2006). These expression profiles are of no value for expression analysis and were removed from the data set; only expression profiles that were highly reproducible (Pearson's correlation, $P < 0.05$) across the two strains were kept for further analysis. In this manner, 955 TDFs were selected and used for adaptive quality-based clustering (De Smet et al., 2002). With high-stringency settings (see "Materials and Methods"), 917 TDFs were grouped in nine expression clusters (designated C1–C9; Supplemental Fig. S7). Figure 6 shows the expression patterns of all these TDFs during the cell cycle of both genotypes by hierarchical clustering (Eisen et al., 1998). TDFs in clusters C1 and C2 had their maximal expression during darkness (0 h), and the level of expression decreased drastically within the first few hours after darkness. Expression of TDFs in clusters C3 and C4 was induced after illumination, peaking at 2 and 3 h, respectively, after darkness. Average peak expression in cluster C5 occurred at 4 to 6 h after darkness, corresponding with the initiation of chloroplast division and the appearance of the first dividing cells. This cluster contained all identified TDFs with nucleotide-binding regions (Table I). Two of these were the universal S-phase-specific genes, histone H3 and MCM5. Histone H3 (Sr025; Kapros et al., 1992; Menges et al., 2002) was maximally expressed at 7 h (Supplemental Fig. S8). The universal DNA replication licensing factor MCM5 (Sr027) had a discrete expression at 4 h. This latter gene is specifically involved in the initiation of DNA synthesis and unwinding of the DNA at the replication forks and has been shown to be temporally expressed at the G1/S transition (Tsuruga et al., 1997; Takisawa et al., 2000). Therefore, the expression of the MCM5 ortholog represents a good marker for S-phase initiation and was used to demarcate the G1 and S phases during synchronization. While genes in cluster C6 were discretely expressed at 7 h, genes in cluster C7 had a broader expression range. They were induced at 6 h, in correspondence with the first occurrences of dividing cells, until the 12th h at the moment of cell separation. Genes in this cluster were expressed simultaneously with the enrichment of G2-phase cells and dividing cells. They consisted of an early and late expression subgroup, indicated as C7-Early (C7-E), containing genes induced at 6 h, and C7-Late (C7-L), containing genes induced at 8 h. Clusters C8 and C9 comprised a rather small number of expression profiles, peaking at three (3, 7, and 10–12 h) and two (0 and 12 h) nonconsecutive time points, respectively.

In total, 378 TDFs (41%) with reproducible expression profiles across the two genotypes were selected for sequencing. Since we were interested primarily in the progression of the cell cycle, proportionally more TDFs were selected from clusters C5 and C7, in which expression was up-regulated after reillumination (Supplemental Table S2). Good-quality sequences were found in 322 TDFs (85%), of which 100 had significant (E-value $< 10^{-3}$) similarity (Table I) with

genes in the in-house-constructed database (see "Materials and Methods"). Expression patterns of these annotated TDFs are presented in Supplemental Figure S9. Seventy-two TDFs showed homology with a gene with a putative allocated function, 18 were homologous with sequences without an allocated function (hypothetical proteins), and 10 TDFs matched with diatom orphan genes, for which no homologous counterparts exist (Table I). These latter genes were all confined to the late phases of the cell cycle, indicating that diatom-specific genes might be functionally associated with mitosis and cell separation. Based on the gene homology and the mapping of Gene Ontology (GO) labels and InterPro domains (see "Materials and Methods"; Supplemental Tables S3 and S4), the TDFs with annotated functions were classified into 11 distinct functional groups (Table I).

Modulated Expression of Genes Implicated in Cell Metabolism

The majority of the GO-labeled TDFs were active in cellular and metabolic processes (Supplemental Fig. S10). TDFs involved in protein biosynthesis were dominant in S-phase cluster C5. Two genes were found to be involved in amino acid synthesis, namely N-acetyl-γ-glutamyl-phosphate reductase (Sr029) and the bifunctional ATP sulfurylase-adenosine 5'-phosphosulfate kinase (Sr033). Various components of the translation machinery dominated this cluster: three TDFs encoded ribosomal proteins (Sr030, Sr031, and Sr032) and one encoded an aspartyl-tRNA synthetase (Sr034). A translation initiation factor 3 (Sr050) was induced shortly after these genes, in cluster C7-E. In addition, nine posttranslational modification proteins were identified (Sr001, Sr002, Sr009, Sr010, Sr028, Sr047, Sr048, Sr049, and Sr073). Four of these genes were expressed in cluster C7-E but two of them, a ClpX homolog (Sr001; Weart et al., 2005) and a ubiquitin-conjugating enzyme (Sr002), were highly expressed in the G1-phase cluster C2 when cells were released from the dark and were rapidly down-regulated after the first hour of light. A series of hypothetical proteins with undefined function displayed an identical regulation.

Several genes of the chloroplast-localized fatty acid biosynthetic pathways (Ohlrogge and Browse, 1995) were modulated during different phases of the cell cycle. β-Hydroxyacyl-ACP-dehydratase (Sr023) was identified in cluster C5, while two fatty acid desaturases (Sr044 and Sr045) were expressed some time later in cluster C7-E. Transcription of glycerol-3-phosphate dehydrogenase (Sr091), also referred to as dihydroxyacetone phosphate reductase (Gee et al., 1988), was activated during cell separation in cluster C9, starting 10 h after reillumination.

To drive the anabolic pathways of protein and fatty acid synthesis, the cell depends on an acetyl-CoA pool, which can be produced by the aerobic oxidation of carbohydrates (Fernie et al., 2004). In this respect, the
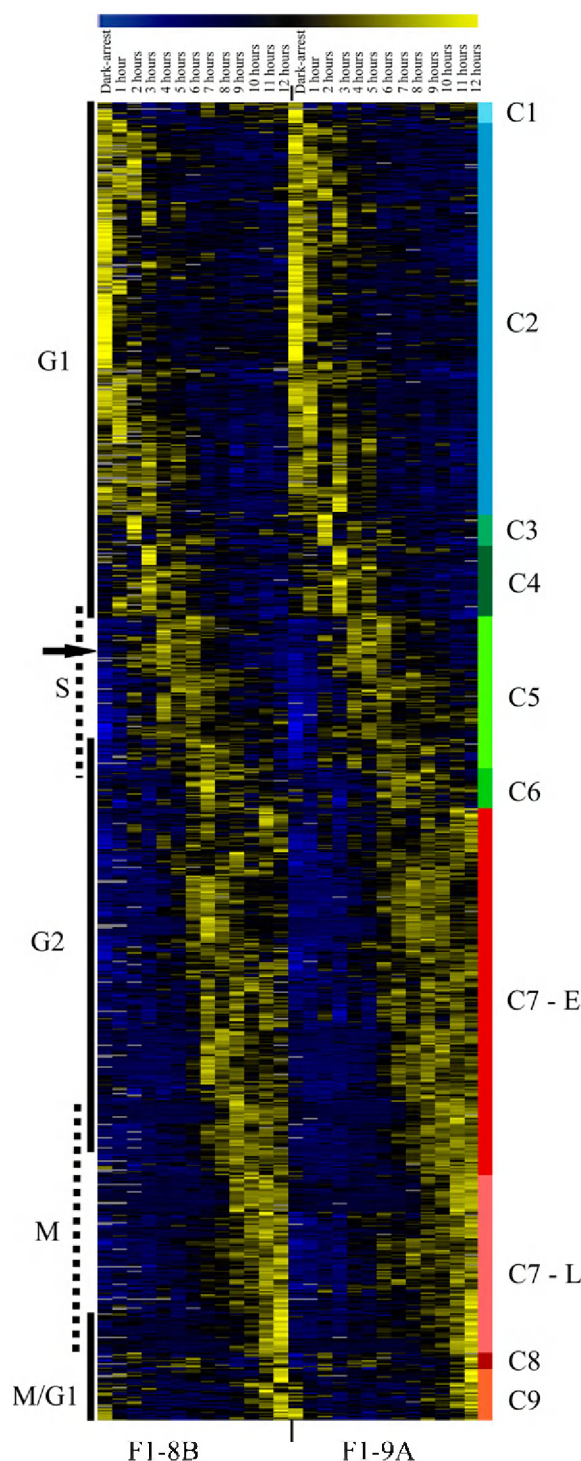
Figure 6. Hierarchical clustered expression profiles of 917 TDFs reproducibly modulated during the cell cycle of synchronized cultures of strain F_1-8B and F_1-9A. Clustering was performed using TMEV software (Saeed et al., 2003) and the hierarchical clustering algorithm (Eisen et al., 1998). Each row represents a tag with the relative transcript accumulation patterns shown over 12 consecutive time points (columns) after reillumination of dark-arrested cultures. Yellow and blue color intensities reflect up- and down-regulation of gene expression relative to a range of +3 to –3, respectively; gray represents missing data. Cluster names (in accordance with adaptive quality-based clus-

glycolytic enzyme enolase (Sr017) was expressed in cluster C5 together with the mitochondrion-localized enzyme isocitrate dehydrogenase (Sr015) and a mitochondrial phosphate-carrier protein (Sr016), both needed during active citric acid cycling.

Two TDFs (Sr051 and Sr095), a subunit of the vacuolar (V)-type H^+-ATPase and a V-type H^+-pyrophosphatase, are known to play a role in vacuolar transport. More particularly, they are responsible for the acidification or maintenance of the acidity of organelles (Maeshima, 2001). Sr051 was activated during G2/M phase in cluster C7-E, while Sr095 was initially expressed slightly during darkness and again abundantly during cell separation (cluster C9).

Modulated Expression of Photosynthesis-Related Genes and Genes Involved in Chloroplast Movement

Fifteen TDFs were assigned to the functional category of photosynthesis (Table I). Using a χ^2 correlation test (Supplemental Table S5), this functional category was found to be dominantly expressed ($P < 0.001$) in cluster C7-L: one TDF was found in C7-E and two in C9. Nine copies of the chromophyte-specific fucoxanthin-chlorophyll a/c-binding proteins (FCPs; Green and Durnford, 1996) were identified, and they were complemented with four TDFs involved in the biosynthesis of their bound photosynthetic pigments: porphobilinogen synthase (Sr063), protoporphyrinogen IX oxidase (Sr068), and protoporphyrin IX magnesium chelatase subunit H (Sr046). They all encoded enzymes from the chlorophyll a/c biosynthetic pathway (von Wettstein et al., 1995). In addition, a ζ-carotene desaturase (Sr062) was identified, being an intermediate enzyme in the biosynthetic pathway of β-carotene and other carotenoids, such as fucoxanthin (Wilhelm et al., 2006). Several Calvin cycle enzymes were also expressed in C7-L and C9: phosphoribulokinase (Sr070), transketolase (Sr093), and glyceraldehyde-3-phosphate dehydrogenase (Sr089). However, because glyceraldehyde-3-phosphate dehydrogenase is also an enzyme involved in glycolysis, it was assigned to the functional category of carbohydrate metabolism. Four genes operating in reactive oxygen metabolism were found in cluster C7-L: one TDF (Sr074) was highly similar to manganese superoxide dismutase (SOD; Wolfe-Simon et al., 2006), and three TDFs (Sr075, Sr076, and Sr077) were highly similar to the peroxisomal membrane protein MPV17/PMP22, which is known to up-regulate the activity of SODs in animal cells (Iida et al., 2003). These genes probably relate to photosynthetic reactive oxygen species generation, which is an inevitable part of oxygenic photosynthesis (Horton et al., 1996; Apel and Hirt, 2004).

tering) and cell cycle phases are indicated at right and left, respectively. The arrow corresponds with the expression profile of the DNA replication licensing factor MCM5.

Table I. *Identified cell cycle-modulated genes with significant E value (<0.001)*

No.	Cluster	Protein Name	Functional Category	Accession No.	E Value	Percent Identity	Length (Amino Acids)
Sr001	C2	ClpX, ATPase regulatory subunit	Posttranslational modification	11217 (Phatr v2.0)	5.0E-26	86.3	67
Sr002	C2	Ubiquitin-conjugating enzyme	Posttranslational modification	CAL55210	2.0E-17	41.1	175
Sr003	C2	Rab6 protein	Signal transduction mechanisms	21535 (Phatr v2.0)	6.0E-18	64.4	96
Sr004	C2	Hypothetical protein	Unknown	ZP_00949502	7.0E-09	69	67
Sr005	C2	Hypothetical protein	Unknown	CAF23694	2.0E-08	31.5	111
Sr006	C2	Hypothetical protein	Unknown	49931 (Phatr v2.0)	5.0E-09	30.4	111
Sr007	C2	Hypothetical protein	Unknown	49931 (Phatr v2.0)	2.0E-07	30.2	101
Sr008	C2	Protein involved in flagellar biosynthesis	Unknown	YP_001100159.1	3.0E-57	61.7	179
Sr009	C4	Ubiquitin	Posttranslational modification	3414 (Thaps v3.0)	4.0E-06	40.2	392
Sr010	C4	N-Ethylmaleimide-sensitive factor	Posttranslational modification	12620 (Phatr v2.0)	6.0E-12	72.9	83
Sr011	C4	Hypothetical chloroplast protein PhtrCp016	Unknown	YP_874373.1	4.0E-06	52.3	48
Sr012	C4	Hypothetical chloroplast protein PhtrCp016	Unknown	YP_874373.1	2.0E-19	77.3	67
Sr013	C4	Hypothetical chloroplast protein PhtrCp016	Unknown	YP_874373.1	2.0E-23	72.3	66
Sr014	C4	Hypothetical protein with DUF1349	Unknown	36940 (Phatr v2.0)	3.0E-50	48.5	198
Sr015	C5	Isocitrate dehydrogenase NADP-dependent, monomeric type	Carbohydrate metabolism	45017 (Phatr v2.0)	2.0E-12	69.5	83
Sr016	C5	Mitochondrial phosphate carrier protein	Carbohydrate metabolism	27276 (Thaps v3.0)	4.0E-45	82.4	116
Sr017	C5	Enolase	Carbohydrate metabolism	40391 (Thaps v3.0)	1.0E-58	85.6	137
Sr018	C5	WD40-repeat protein	Cytoskeleton	48381 (Phatr v2.0)	3.0E-14	52.1	106
Sr019	C5	β-Tubulin	Cytoskeleton	21122 (Phatr v2.0)	2.0E-30	80.4	105
Sr020	C5	Aldo/keto reductase	Electron transport	51714 (Phatr v2.0)	8.0E-12	42.1	122
Sr021	C5	Thioredoxin family protein	Electron transport	43106 (Phatr v2.0)	4.0E-07	57.1	65
Sr022	C5	Flavodoxin	Electron transport	19141 (Thaps v3.0)	3.0E-30	73.5	211
Sr023	C5	β-Hydroxyacyl-ACP dehydratase precursor	Fatty acid metabolism	55157 (Phatr v2.0)	3.0E-48	84.1	114
Sr024	C5	RNA or DNA helicase	Nucleotide binding	21388 (Phatr v2.0)	3.0E-25	68.4	91
Sr025	C5	Histone H3	Nucleotide binding	3183 (Thaps v3.0)	4.0E-34	100	80
Sr026	C5	Protein with helicase region	Nucleotide binding	3158 (Thaps v3.0)	1.0E-11	44.8	112
Sr027	C5	Minichromosome maintenance-deficient protein 5 (MCM 5)	Nucleotide binding	11490 (Phatr v2.0)	7.0E-28	60	116
Sr028	C5	Chaperonin-containing TCP1, subunit 2 (CCT2)	Posttranslational modification	33432 (Thaps v3.0)	9.0E-46	72.6	158
Sr029	C5	N-Acetyl-γ-glutamyl-phosphate reductase	Protein synthesis	36913 (Phatr v2.0)	2.0E-23	78.2	75
Sr030	C5	60S ribosomal protein L3	Protein synthesis	13361 (Phatr v2.0)	1.0E-43	87.7	107
Sr031	C5	60S ribosomal protein L3	Protein synthesis	13361 (Phatr v2.0)	2.0E-35	89	88
Sr032	C5	Ribosomal protein L32	Protein synthesis	21659 (Phatr v2.0)	2.0E-15	70.4	110
Sr033	C5	Bifunctional ATP sulfurylase/adenosine 5'-phosphosulfate kinase	Protein synthesis	19901 (Phatr v2.0)	5.0E-17	61.9	75
Sr034	C5	Aspartyl-tRNA synthetase	Protein synthesis	42051 (Phatr v2.0)	1.0E-53	81.1	123
Sr035	C5	TonB-dependent receptor	Signal transduction mechanisms	ZP_01060962.1	8.0E-07	63	129
Sr036	C5	Hypothetical protein, conserved	Unknown	21905 (Thaps v3.0)	2.0E-23	75.3	158
Sr037	C5	Hypothetical protein	Unknown	20641 (Thaps v3.0)	6.0E-07	35.5	111
Sr038	C5	Membrane-spanning protein (nonaspanin family)	Unknown	268610 (Thaps v3.0)	3.0E-17	77.7	72
Sr039	C6	Leu-rich repeat-like protein	Signal transduction mechanisms	5595 (Thaps v3.0)	1.0E-06	41.4	155
Sr040	C6	Receptor guanylyl cyclase GC-II	Signal transduction mechanisms	36270 (Phatr v2.0)	1.0E-10	88.2	36
Sr041	C6	Orphan gene	Unknown	48715 (Phatr v2.0)	3.0E-22	41.8	117

(Table continues on following page.)

Table I. (Continued from previous page.)

No.	Cluster	Protein Name	Functional Category	Accession No.	E Value	Percent Identity	Length (Amino Acids)
Sr042	C7-E	GDP-Man 4,6-dehydratase	Carbohydrate metabolism	25417 (Phatr v2.0)	1.0E-11	61.1	60
Sr043	C7-E	Glutathione S-transferase	Electron transport	NP_104774.1	5.0E-09	37.6	114
Sr044	C7-E	C5 sterol desaturase	Fatty acid metabolism	37371 (Phatr v2.0)	1.0E-13	61.1	67
Sr045	C7-E	δ-9-Desaturase	Fatty acid metabolism	28797 (Phatr v2.0)	5.0E-06	52.5	65
Sr046	C7-E	Protoporphyrin IX magnesium chelatase, subunit H	Photosynthesis	13265 (Phatr v2.0)	3.0E-20	95.9	54
Sr047	C7-E	26S protease regulatory subunit	Posttranslational modification	264206 (Thaps v3.0)	7.0E-66	93.8	145
Sr048	C7-E	Metalloproteinase	Posttranslational modification	ZP_01984772	3.0E-16	40	154
Sr049	C7-E	Prolylcarboxypeptidase	Posttranslational modification	29166 (Thaps v3.0)	7.0E-13	48.1	121
Sr050	C7-E	Eukaryotic translation initiation factor 3	Protein synthesis	35933 (Thaps v3.0)	9.0E-16	42.1	120
Sr051	C7-E	V-type H$^+$-ATPase subunit DVA41	Transport protein	21030 (Phatr v2.0)	6.0E-24	86.6	61
Sr052	C7-E	Hypothetical protein	Unknown	10781 (Phatr v2.0)	3.0E-16	56.8	111
Sr053	C7-E	Hypothetical protein	Unknown	12740 (Phatr v2.0)	1.0E-16	58.8	94
Sr054	C7-E	Hypothetical protein	Unknown	45678 (Phatr v2.0)	6.0E-11	84.2	91
Sr055	C7-E	Orphan gene	Unknown	32962 (Phatr v2.0)	9.0E-16	97.4	45
Sr056	C7-E	Hypothetical protein	Unknown	EAU80690.1	3.0E-04	28.9	135
Sr057	C7-L	Succinate/fumarate mitochondrial transporter	Carbohydrate metabolism	23709 (Phatr v2.0)	2.0E-69	79.7	161
Sr058	C7-L	Alcohol oxidase-related protein	Electron transport	48204 (Phatr v2.0)	1.0E-13	50	110
Sr059	C7-L	Cytochrome P450	Electron transport	43467 (Phatr v2.0)	6.0E-05	44	107
Sr060	C7-L	Myoinositol dehydrogenase	Electron transport	1049 (Thaps v3.0)	7.0E-76	73.6	188
Sr061	C7-L	Fucoxanthin-chlorophyll a/c-binding protein	Photosynthesis	CAA04401	1.0E-28	85.2	108
Sr062	C7-L	ζ-Carotene desaturase (ZDS)	Photosynthesis	9040 (Phatr v2.0)	1.0E-37	92.6	84
Sr063	C7-L	Porphobilinogen synthase	Photosynthesis	YP_984596.1	3.0E-47	89.7	108
Sr064	C7-L	Fucoxanthin-chlorophyll a/c-binding protein	Photosynthesis	CAA05142.1	4.0E-11	83.3	39
Sr065	C7-L	Light-harvesting protein	Photosynthesis	270092 (Thaps v3.0)	4.0E-06	85	69
Sr066	C7-L	Light-harvesting protein	Photosynthesis	14648 (Phatr v2.0)	2.0E-24	76	102
Sr067	C7-L	Fucoxanthin-chlorophyll a/c-binding protein	Photosynthesis	CAA04401	3.0E-32	83	107
Sr068	C7-L	Protoporphyrinogen IX oxidase	Photosynthesis	264901 (Thaps v3.0)	6.0E-46	64.1	186
Sr069	C7-L	Fucoxanthin-chlorophyll a/c-binding protein	Photosynthesis	CAA04401	1.0E-32	85.3	107
Sr070	C7-L	Phosphoribulokinase	Photosynthesis	10208 (Phatr v2.0)	3.0E-43	87.6	126
Sr071	C7-L	Fucoxanthin-chlorophyll a/c-binding protein	Photosynthesis	CAA04401.1	6.0E-57	69.2	194
Sr072	C7-L	Fucoxanthin-chlorophyll a/c-binding protein	Photosynthesis	22395 (Phatr v2.0)	5.0E-33	81.8	113
Sr073	C7-L	Peptidylprolyl cis/trans-isomerase	Posttranslational modification	1989 (Thaps v3.0)	5.0E-10	48	67
Sr074	C7-L	Superoxide dismutase 1 (SOD1)	Reactive oxygen species metabolism	12583 (Phatr v2.0)	3.0E-45	91	89
Sr075	C7-L	Peroxisomal membrane protein MPV17/PMP22	Reactive oxygen species metabolism	12379 (Phatr v2.0)	3.0E-16	88.8	116
Sr076	C7-L	Peroxisomal membrane protein MPV17/PMP22	Reactive oxygen species metabolism	12379 (Phatr v2.0)	1.0E-15	95.1	98
Sr077	C7-L	Peroxisomal membrane protein MPV17/PMP22	Reactive oxygen species metabolism	12379 (Phatr v2.0)	1.0E-06	89.6	54
Sr078	C7-L	Flagellin-sensing 2-like protein	Signal transduction mechanisms	NP_001043191.1	2.0E-06	40.2	77

(Table continues on following page.)

Table I. *(Continued from previous page.)*

No.	Cluster	Protein Name	Functional Category	Accession No.	E Value	Percent Identity	Length (Amino Acids)
Sr079	C7-L	Ser/Thr protein kinase and signal transduction histidine kinase (STHK) with GAF sensor	Signal transduction mechanisms	48535 (Phatr v2.0)	1.0E-26	35.2	274
Sr080	C7-L	Hypothetical protein	Unknown	24150 (Thaps v3.0)	1.0E-08	46	168
Sr081	C7-L	Hypothetical protein	Unknown	32401 (Phatr v2.0)	4.0E-21	49.1	162
Sr082	C7-L	Orphan gene	Unknown	22117 (Thaps v3.0)	7.0E-28	53.9	112
Sr083	C7-L	Orphan gene	Unknown	4807 (Thaps v3.0)	3.0E-28	51.3	127
Sr084	C7-L	Hypothetical protein	Unknown	50021 (Phatr v2.0)	5.0E-07	509	55
Sr085	C7-L	Orphan gene	Unknown	20812 (Thaps v3.0)	1.0E-04	90.4	36
Sr086	C7-L	Orphan gene	Unknown	3345 (Thaps v3.0)	7.0E-04	36.8	81
Sr087	C8	5'-Adenylylsulfate reductase, chloroplast precursor	Electron transport	10518 (Phatr v2.0)	1.0E-41	68.8	125
Sr088	C8	Hypothetical protein	Unknown	15801(Phatr v2.0)	8.0E-23	35.5	178
Sr089	C9	Glyceraldehyde-3-phosphate dehydrogenase	Carbohydrate metabolism	22122 (Phatr v2.0)	6.0E-17	93.2	46
Sr090	C9	Cytochrome P450 3A10	Electron transport	43467 (Phatr v2.0)	5.0E-05	44	98
Sr091	C9	Glycerol-3-phosphate dehydrogenase	Fatty acid metabolism	40073 (Thaps v3.0)	5.0E-51	75	135
Sr092	C9	Fucoxanthin-chlorophyll *a/c*-binding protein	Photosynthesis	22395 (Phatr v2.0)	8.0E-33	52.7	176
Sr093	C9	Transketolase	Photosynthesis	29260 (Phatr v2.0)	2.0E-39	63.1	126
Sr094	C9	Leu-rich repeat receptor protein	Signal transduction mechanisms	45913 (Phatr v2.0)	7.0E-15	40	167
Sr095	C9	V-type H^+-pyrophosphatase	Transport protein	CAL50249.1	2.0E-11	55.9	174
Sr096	C9	Sodium/calcium exchanger family protein	Transport protein	31322 (Phatr v2.0)	6.0E-44	74.4	154
Sr097	C9	Orphan gene	Unknown	49286 (Phatr v2.0)	1.0E-13	80.9	59
Sr098	C9	Orphan gene	Unknown	49286 (Phatr v2.0)	3.0E-23	86.4	64
Sr099	C9	Orphan gene	Unknown	268304 (Thaps v3.0)	4.0E-10	44.7	115
Sr100	C9	Orphan gene	Unknown	37765 (Phatr v2.0)	5.0E-31	40.5	201

β-Tubulin (Sr019), which plays a fundamental role in cytoskeleton-based cellular movements, was highly induced 4 h and maximally expressed 6 h after darkness. This induction (clustered within C5) slightly preceded chloroplast reorganization. Another TDF with similarity to a WD40-repeat protein (Sr018), putatively involved in cytoskeleton assembly, was analogously expressed; both genes were down-regulated 6 h after darkness but β-tubulin was again slightly induced at 8 h, in parallel with cell division (Supplemental Fig. S11). The involvement of microtubule-based cytoskeleton dynamics during chloroplast movement was expected and further validated by treatment of synchronized cultures with the microtubule inhibitor nocodazole. Nine hours after treatment, chloroplast division and reorganization were impaired when compared with untreated control cultures. Only after 26 h did chloroplast division and reorganization proceed, arresting the cells at G2+M phase (data not shown).

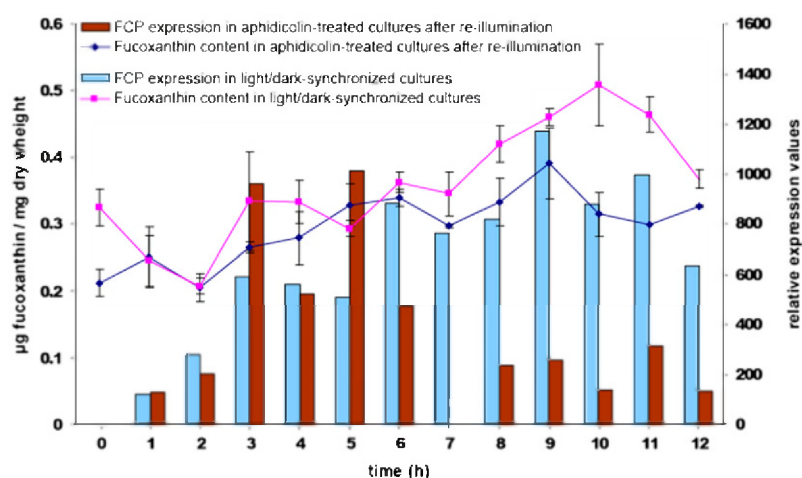### Cell Cycle versus Light Regulation of Photosynthesis and Pigment Biosynthesis

The microscopic observations (Fig. 4) showed that chloroplasts elongated after cell division initiation when they relocated to the girdle sides of the cell. To investigate whether this elongation is paralleled with chloroplast growth, we determined fucoxanthin pigment turnover and validated the FCP expression with RT-Q-PCR in synchronized cultures. In addition, these data were compared with those from synchronized cultures to which the cell cycle inhibitor aphidicolin had been added shortly before reillumination (Fig. 7). This was done to assess the dependence of pigment turnover and FCP expression on cell cycle progression versus light regulation.

Upon reillumination, fucoxanthin content per cell increased under both conditions, but the trend was more pronounced in the dividing cultures than in the S-phase-arrested cultures. This fucoxanthin accumulation in the dividing cultures was obvious after 5 h of light and decreased after 10 h, corresponding with cell separation (Fig. 3). In the S-phase-arrested cultures, the accumulation curve was more gradual, without a clear peak and with a smaller maximum. Although the difference between both profiles was obvious, a longitudinal ANOVA test was unable to prove its significance, which could be due to the small number of replicates.

In parallel, in response to reillumination in both cultures, FCP expression was activated and subsequently down-regulated after 5 h in the arrested cultures, whereas in cell cycle-progressing cultures, its expression was maintained throughout the 13-h time course (Fig. 7). These findings suggest that

Figure 7. Comparison of fucoxanthin pigment turnover and *FCP* expression between light/dark-synchronized cultures and light/dark-synchronized cultures to which the cell cycle inhibitor aphidicolin was added shortly before reillumination. A difference in fucoxanthin pigment (μg mg^{-1} dry weight) accumulation is apparent after 5 h of reillumination. In the S-phase-arrested cultures, the buildup is less pronounced. In parallel, *FCP* expression is up-regulated between 1 and 5 h after reillumination in both dividing and arrested cultures, but its expression is down-regulated after the initial increase in arrested cultures while it is maintained in the dividing cultures. [See online article for color version of this figure.]

DISCUSSION

Regulation of Chloroplast Dynamics with Respect to Cell Cycle Progression and Frustule Silicification

In diatoms, chloroplast division and development have not yet been considered in relation to cell cycle regulation. For example, darkness was shown to arrest the cell cycle in several diatom species (Vaulot et al., 1986; Brzezinski et al., 1990), but microscopic observations of the effect on chloroplasts are, to our knowledge, completely lacking. A putative reason is that mostly polyplastidic centric diatoms have been studied in which the small chloroplasts are stochastically partitioned upon cell division and, hence, have not such an obvious developmental cycle. In addition, the fact that flow cytometry is traditionally preferred to investigate cell cycle effects might have contributed to the general neglect of morphology and cytology.

As shown here for the pennate diatom *S. robusta*, chloroplast division and development are intimately linked with cell cycle progression. First, conditions that activate the G1-to-S cell cycle checkpoint (i.e. light deprivation, HU, or aphidicolin) arrest the development of chloroplasts at the plastokinesis stage without inducing aberrant cell morphologies. Second, both divided chloroplasts rotate from the girdle to the valves before karyokinesis is initiated. And, at last, the chloroplast division homolog *FtsZ* is expressed in concert with chloroplast division in a cell cycle phase-dependent manner, during the S/G2 phases. We conclude that the G1-to-S-checkpoint controls chloroplast division and relocation and enables their synchronous division in *S. robusta* cultures. Previous observations of chloroplast dynamics during the cell cycle in *S. robusta*

had already shown that chloroplasts and the nucleus divide in a coordinated manner (Chepurnov et al., 2002). Now, we observe that both also depend on each other and that common mechanisms to regulate their division should be involved. Similarly, in the red alga *Cyanidioschyzon merolae*, chloroplast and mitochondrion divisions are regulated at distinct cell cycle checkpoints (Nishida et al., 2005). However, in contrast with aphidicolin-arrested *S. robusta* cells, in *C. merolae* the mitochondrial division is restrained while the chloroplast divides multiple times (Itoh et al., 1996; Nishida et al., 2005).

Since its initial discovery in Arabidopsis (*Arabidopsis thaliana*; Osteryoung and Vierling, 1995), homologs of the bacterial cell division protein FtsZ are held responsible for organelle division in many other eukaryotes (Beech and Gilson, 2000; Takahara et al., 2000; Kiefel et al., 2004) that occurs by FtsZ assembling into the bacterial cytokinetic apparatus, called the Z-ring (Osteryoung and Nunnari, 2003; Margolin, 2005). Accordingly, *FtsZ* expression is modulated during synchronized growth of tobacco (*Nicotiana tabacum* BY2; El-Shami et al., 2002) and *C. merolae* (Takahara et al., 2000; Nishida et al., 2005), in a circadian rhythm in *Chlamydomonas reinhardtii* (Hu et al., 2008), and in light/dark-synchronized cultures of *S. robusta* as well. Its expression is up-regulated after S-phase progression and prior to cell division, in agreement with microscopic observations. This shows that the chloroplast developmental cycle can be monitored unmistakably through synchronization of cell division in *S. robusta*.

Control of chloroplast division is governed by conserved cell cycle regulators of bacterial origin (Adams et al., 2008). One of these, the chaperone ClpX, identified here, was down-regulated upon reillumination when cells reentered the cell cycle. ClpX has been found to inhibit Z-ring formation in *Bacillus subtilis* (Weart et al., 2005). It is tempting, therefore, to suggest that the activation of *ClpX* in a dark-arrested cell ensures the inhibition of plastokinesis in *S. robusta*.

chloroplast growth occurs in advance of chloroplast elongation at cytokinesis, while chloroplast light-harvesting complexes are regulated by both the cell cycle and light.

Another resemblance can be found with the regulation of plastokinesis at the G1/S transition in Arabidopsis (Raynaud et al., 2005), in which chloroplast division was regulated by the activity of the prereplication factor CDT1. In *S. robusta*, chloroplast division was paralleled by activation of the S-phase-specific gene *MCM5*, which is also a universal member of the prereplication complex. Furthermore, our observations also suggest that "retrograde" mechanisms (Koussevitzky et al., 2007), which involve signaling from the chloroplast to the nucleus, might be present as another way to coordinate the chloroplast and nuclear division cycle. Retrograde signaling was, for example, reported in response to membrane tension as a possible way to regulate shape, size, and division of chloroplasts in Arabidopsis (Haswell and Meyerowitz, 2006). Analogous feedback mechanisms might exist within diatoms, for example, to control the G2/M transition in response to the chloroplast developmental status, ensuring high-quality chloroplast segregation of daughter chloroplasts to the newly divided cells. In any case, control mechanisms may not be as strict in centric polyplastidic diatoms because, similar to what is known for land plants, a stochastic partitioning of chloroplasts upon cell division will hardly result in cells without any chloroplast (Coleman and Nerozzi, 1999).

The molecular mechanism of chloroplast movement in diatoms is still unclear. In polyplastidic diatoms, the red alga *C. merolae*, and plants, chloroplast movements are known to be actin dependent (de Francisco and Roth, 1977; Nishida et al., 2005; Krzeszowiec et al., 2007). The transcriptional induction of β-tubulin in *S. robusta* suggests the involvement of microtubules during chloroplast rearrangement but does not exclude the possibility that actin may also be involved.

The intriguing question remains why pennate diatoms display this sometimes complicated cycle of repositioning the chloroplast during cell cycle progression. One possibility is that the position of the chloroplasts at the valves might create a disadvantage for cell movement needed for adequate reaction to environmental factors, such as light and nutrients (Cohn and Disparti, 1992). Because cells glide across the surface by mucilage secretion from a valvar slit (called the raphe; Hoagland et al., 1993; Wetherbee et al., 1998; Chiovitti et al., 2006), the underlying actin-myosin system that is held responsible for the raphe's functionality could be impaired by a valvar location of the chloroplasts. In cultures of *S. robusta*, cells with a reorganized chloroplast configuration have indeed never been observed moving. This reasoning was first introduced in Mereschkowsky's "law" on diatom chloroplasts, which states that chloroplasts of diatoms have a tendency to leave the raphe as much as possible uncovered (Mereschkowsky, 1904). This is achieved in numerous diatoms (*Brebissonia* spp., *Cymbella* spp., *Gomphonema* spp., *Dickieia ulvacea*, *Didymosphenia* spp., and *Lyrella* spp.) by plastid invaginations beneath the raphe (Mann, 1996), whereas in other diatoms, such as

S. robusta, it is achieved by positioning of the chloroplasts at the valves only during a short time of the cell cycle. As observed here, this positioning at the valves is necessary only to free the girdle area for the addition of girdle bands, cytokinesis, and frustule formation. The identified girdle bands were indeed observed late during the cell cycle, in cells with a reorganized chloroplast configuration. As such, the cyclic movement of chloroplasts could create a large enough time frame for a cell to position itself optimally within the environment, maximally favoring cell growth, before cell division is committed. It is an interesting speculation that because centric diatoms are planktonic, lack a raphe, and are thus unable to move, they did not evolve such a well-orchestrated chloroplast development cycle. Also, variations in the chloroplast cycle in diatoms might explain the differences in the timing of girdle band deposition among species (Coombs et al., 1967b; Chiappino and Volcani, 1977; Kröger and Wetherbee, 2000; Hildebrand et al., 2007). For example, *T. pseudonana*, which is polyplastidic, was shown recently to synthesize its girdle bands already during G1 phase (Hildebrand et al., 2007).

Girdle bands accommodate cell growth and, like frustules, are formed by polymerization of silica in a silica deposition vesicle (SDV) that is exocytosed (Pickett-Heaps et al., 1990; Kröger and Wetherbee, 2000; Zurzolo and Bowler, 2001). Not much is known about the origin of the SDV, but it probably originates from other internal vesicle compartments, such as the endoplasmic reticulum, Golgi, and lysosome (Lee and Li, 1992). In this regard, the TDF Sr051, identified as a subunit of the V-type H^+-ATPase, is of particular interest because such energy-consuming proton transport proteins have a known functionality in the acidification of organelles (Maeshima, 2001). It was maximally expressed 1 h before the initiation of cell separation (at 8 h after darkness), when the two "vacuole-like" compartments also were visible by PDMPO accumulation. Because diatom silicification occurs inside an acidic SDV (Mayama and Kuriyama, 2002), the V-type H^+-ATPase could be related to girdle or valve formation at the stage of SDV acidification. A P-type ATPase was recently also hypothesized to be involved in SDV formation, during expansion of its plasma membrane in *T. pseudonana* (Frigeri et al., 2006). Possibly, both identified V-type and P-type ATPases are required in parallel during valve formation in diatoms.

Cell Cycle Synchronization of *S. robusta*

In many studies using phytoplankton cultures (for review, see Pirson and Lorenzen, 1966; Tamiya, 1966; Krupinska and Humbeck, 1994), the endogenous cell cycle control mechanisms that respond to naturally phased light/dark conditions are exploited to study cell division in synchronous cultures (Otero and Goto, 2005). Diatoms are known to be capable of sustaining long periods of darkness and retain the ability to start

growing rapidly upon reillumination (Furusato et al., 2004). The synchronization protocol established here for *S. robusta* relies on this apparently fast release from the dark-arrested G1 phase. As a result of the identified common regulatory mechanisms in chloroplast division and cell cycle progression, this procedure was found successful for studying both processes simultaneously.

The uniformly dark-induced G1-phase arrest in *S. robusta* appears unusual when compared with other diatoms. The centric diatom *Thalassiosira weissflogii* accumulates, besides G1-phase cells, 60% G2+M-phase cells (Olson et al., 1986; Vaulot et al., 1986; Brzezinski et al., 1990), and other centric diatoms (*Chaetoceros muellerii*, *T. pseudonana*, *Chaetoceros simplex*, and *Minutocellus polymorhus*) plus one pennate diatom (*Cylindrotheca fusiformis*) all accumulate G1-phase cells together with a smaller fraction (approximately 10%) of G2+M-phase cells (Brzezinski et al., 1990). The pennate diatom *P. tricornutum* is the only diatom reported without a dark-sensitive G2+M phase, and its facultative silicon requirement has been put forward as the main reason for this observation (Brzezinski et al., 1990). However, in diatoms, the G2+M-phase fraction in flow cytometric signatures includes, besides G2- and M-phase cells, also postcytokinetic doublet cells, which have completed cell wall formation but have not yet separated. Therefore, the "G2+M-phase" fraction in the dark-arrest experiment by Brzezinski et al. (1990) might have been postcytokinetic doublet cells. In *S. robusta*, the occasionally detected G2+M-phase cells at 24 h of dark arrest were microscopically observed to be all postcytokinetic doublet cells containing girdle-located chloroplasts, typical for G1-phase cells. Apparently, only the process of cell separation and not cytokinesis is hampered in these cells by the absence of light. Therefore, we suggest that it might be useful to address cell separation in diatoms analogously as in yeast cells, where it is defined as a postmitotic phase and known to be molecularly distinct from the septum formation process during M phase (Yeong, 2005; Sipiczki, 2007).

Based on the expression of the prereplication factor MCM5 and the occurrence of dividing chloroplasts, the duration of the G1 phase in *S. robusta* can be estimated to last for 4 h (33% of the total division time) during synchronization under the applied culture conditions. Since the last 3 h were dominated by separating cells, 5 h (41% of the total division time) are left to fulfill the S, G2, and M phases. Our results suggest that cell division during synchronization occurred faster (<12 h) than during normal exponential growth, even when compared with the highest recorded maximum division rate for *S. robusta*, being 16.6 h per division (approximately 1.5 divisions per day under continuous light at 200 μE). As suggested (Olson et al., 1986; Vaulot et al., 1986), part of the G1 phase might already be accomplished during dark arrest. Taking into account this comment, our microscopically estimated cell cycle stage durations of *S.*

robusta correspond roughly with the flow cytometric estimations from *P. tricornutum*, reported to spend half its cell division time in G1 phase (Brzezinski et al., 1990).

Gene Expression in Relation to Chloroplast Functioning and Photosynthesis

The overall results from the cDNA-AFLP experiment confirm the hypothesis that several biological processes are under temporal transcriptional control during the cell cycle of diatoms, as shown previously in similar studies of higher plants and animals (Cho et al., 2001; Menges et al., 2002; Breyne et al., 2002). One of the most distinct patterns in gene modulation concerns those genes encoding chloroplast proteins, associated with the functioning of chloroplasts during photosynthesis, including light-harvesting proteins, biosynthetic pigment enzymes, and genes coping with oxidative damage. Nearly all of these genes were expressed during G2/M-phase progression and clustered into the expression cluster C7-L. Most notable was the expression of *FCP*, a chromophyte-specific type of light-harvesting protein (Bhaya and Grossman, 1993; Eppard and Rhiel, 1998, 2000; Guglielmi et al., 2005), in concert with cell division.

Regulation of *FCP* expression is known to modulate light harvesting primarily during photoacclimation independent of developmental processes (Falkowski and LaRoche, 1991; Durnford and Falkowski, 1997; Leblanc et al., 1999; Oeltjen et al., 2002, 2004; Siaut et al., 2007). Nevertheless, the cell and life cycle dependence of photosynthesis has been shown in several algae, such as *Scenedesmus* spp. (Post et al., 1985; Kaftan et al., 1999; Tukaj et al., 2003; Setlikova et al., 2005), *Euglena gracilis* (Winter and Brandt, 1986), *Chlorella fusca* (Butko and Szalay, 1985), and *C. fusiformis* (Claquin et al., 2004).

In *S. robusta*, *FCP* expression was found to be light activated in the first place, confirming previous results in centric (Leblanc et al., 1999; Oeltjen et al., 2002, 2004) and pennate (Siaut et al., 2007) diatoms. But after 5 h, its expression became cell cycle dependent, because it was maintained in dividing cultures while being repressed in S-phase-arrested cultures. A possible molecular mechanism to explain this difference relates to the retrograde inhibition of light-harvesting proteins known in *C. reinhardtii* and Arabidopsis. In these organisms, light-induced expression of light-harvesting proteins is repressed by accumulation of the chlorophyll precursor Mg-protoporphirin IX (Johanningmeier and Howell, 1984; Nott et al., 2006). Its accumulation, leakage from the chloroplast, and nuclear repression of photosynthetic genes are thought to occur during reduced chloroplast function to coordinate pigment biosynthesis with the expression of light-harvesting proteins (Nott et al., 2006). In an analogous way, if chloroplast development is impaired in *S. robusta*, a retrograde signal might repress *FCP*. The fact that fucoxanthin does not decrease together with *FCP*

could be a result of the low turnover rates of diatom pigments, ranging from days to weeks (Riper et al., 1979; Goericke and Welschmeyer, 1992), compared with the low stability of mRNA.

A recent study by Ragni and Ribera d'Alcalà (2007) on the circadian variations in pigment content in *P. tricornutum* showed that pigment synthesis follows the somatic growth preceding cell division. Furthermore, they observed that a pronounced circadian pattern of pigment synthesis was lost when cultures were continuously illuminated and became asynchronous. This study substantiates our finding that fucoxanthin content increases in preparation of cell division, until it is distributed into daughter cells.

Taking together our microscopic analysis, cDNA-AFLP results, and pigment accumulation patterns, we suggest that cell cycle modulation of photosynthetic light harvesting occurs in concert with chloroplast growth to prepare for its elongation at cytokinesis. Because chloroplasts in *S. robusta* elongate at the stage of cytokinesis, regulated synthesis of more functional light-harvesting complexes would be expected to provide a balanced growth of chloroplasts at this stage, thereby optimizing the cell's photosynthetic capacity during the subsequent G1 phase. Together with light acclimation and circadian regulation, cell cycle-modulated biosynthesis of the large amount of pigments that are contained within diatoms (Chan, 1978, 1980; Falkowski et al., 1985; Tang, 1996) could as such coordinate cellular investments and improve cell fitness.

MATERIALS AND METHODS

Cell Culture and Image Acquisition

The *Seminavis robusta* strains F_1-8B and F_1-9A were selected from a first generation of siblings obtained by crossing the wild-type clones 75 and 80 (Chepurnov et al., 2002). F_1-8B and F_1-9A belong to opposite mating types (Chepurnov et al., 2008) and had at the time of study an average apical cell length of 22.7 ±1.6 and 18.9 ±1.2 μm, respectively. Currently, they are maintained cryopreserved in the culture collection of the Laboratory of Protistology and Aquatic Ecology (http://www.pae.ugent.be/collection.htm). Cell cultures were grown in F/2 medium (Guillard, 1975) made with filtered (GF/C grade microfiber filter; Whatman) autoclaved seawater collected from the North Sea. F/2 nutrients were sterilized through 0.2-μm filters and added to the filtered autoclaved seawater. Na_2SiO_3 was added at a concentration of 30 mg L^{-1} medium. Cultures were cultivated at 18°C with a 12:12-h light:dark period and approximately 85 μmol photons m^{-2} s^{-1} from cool-white fluorescent lights. Stock cultures were reinoculated weekly by transferring small aliquots of cell suspension into fresh medium. Experimental cultures were prepared from stock cultures by inoculating an aliquot of cells from cell suspensions created by scraping the cells from the surface (cell scrapers; Sarstedt) or by detaching the cells by pipetting. Observations and cell culture photography were done with a Zeiss Axiovert 40 light microscope and a digital camera (Powershot G3; Canon). Fluorescence microscopy of cells was performed using Zeiss Axioplan 200, Axiocam MRm for image capturing, and Zeiss filter set 14. Confocal fluorescence images were taken with a laser-scanning confocal microscope (Zeiss Confocal LSM 510) equipped with software package LSM510 version 3.2 (Zeiss) and equipped with a 63× water-corrected objective (numerical aperture 1.2). Chloroplast fluorescence was visualized with helium-neon laser illumination at 543 nm. Nuclear DNA was stained with SYBR Safe (Molecular Probes) that was visualized with argon laser illumination at 488 nm and a 500- to 530-nm band emission filter. Cell walls were stained with the Lysosensor Yellow/Blue DND-160 probe

(PDMPO; Molecular Probes) as described by Leblanc and Hutchins (2005) and visualized by illumination at 351 nm. Emission fluorescence was captured in the line-scanning mode, and for transmission light images, differential interference contrast optics were used.

Cell Cycle Progression Assays and Flow Cytometry

The effect of darkness on cell morphology was tested on exponentially growing cultures of strain F_1-8B (Chepurnov et al., 2008) that were inoculated at 1,000 cells mL^{-1} in tissue culture flasks (Cellstar; 175-cm^2 growth surface with filter screw cap; Greiner Bio-One) with 200 mL of growth medium. After 2 d of growth, the old medium was decanted from the flask-attached cells and the flask was refilled with 200 mL of fresh medium before transferring the cultures to complete darkness to ensure that no nutrient limitation occurred during dark incubation. HU (Fluka) was tested at a final concentration of 6.5 mM, added to 100 mL of exponentially growing cultures of strain F_1-31B. After addition, the cultures were incubated in continuous light during 72 h and compared with blank cultures to which an equal volume of dimethyl sulfoxide was added. The effect of aphidicolin (Sigma-Aldrich; 0.5 μg mL^{-1}) was tested in triplicate on F_1-8B cultures containing approximately 5,000 dark-arrested cells in 10 mL of medium and compared after 24 h of light with dimethyl sulfoxide-treated control cultures.

DNA content was measured on intact fixed cells. Therefore, at least 10 mL of a culture was centrifuged for 10 min at 1,500*g*, and the cells were fixed in 10 mL of ice-cold methanol in the dark at 4°C (Vaulot et al., 1986). Fixed cells were rinsed two to three times with 4 mL of TE (10 mM Tris and 1 mM EDTA, pH 8.0) by centrifugation for 10 min at 1,500*g* and resuspended in 1 mL of TE. Samples were incubated for 40 min at 37°C with 10 μL of 30.5 mg mL^{-1} RNase A (R4642; Sigma-Aldrich) and then placed on ice in the dark. To each sample, 1 μL of 4,6-diamidino-2-phenylindole from a stock of 1 mg mL^{-1} was added, stained for at least 10 min on ice, and filtered over a 50-μm nylon mesh (CellTrics; Partec). The stained cell suspensions were analyzed with a CyFlow flow cytometer and FloMax software (Partec).

Synchronization of *S. robusta* Cells and Sampling of Material

For the synchronization, each *S. robusta* strain was grown in two tissue culture flasks. Because of the difference in cell size, F_1-8B and F_1-9A culture flasks were inoculated with 7.5 × 10^5 and 1 × 10^6 cells, respectively, into 200 mL of medium. Cell density estimates of stock cultures were obtained by microscopically counting cells in a 100-μL aliquot of a suspended culture on a 96-well TC plate. Cultures inoculated for synchronization were grown for 2 d in a 12:12-h light:dark regime. At the end of day 2, the dark period was extended for another 12 h, arresting the cell culture at the G1 phase. A first sample was taken just before the light was switched on, followed by 12 samples taken every hour after reillumination. Just before sampling of each culture, six photographs were taken with the Axiovert 40 microscope and a connected digital camera (Canon Powershot G3). Images were used to count different cell types using the open-source software ImageJ (http://rsb.info.nih.gov/ij/index.html) and the cell counter plug-in. M-phase cells were easily identified and distinguished from interphase cells by the presence of a newly built cell wall, situated between the two valve-located chloroplasts. As soon as daughter cells were separating, they were counted as nondividing cells. In preparation for cell culture harvesting, the cells were concentrated by reducing the medium of the first flask to less than 50 mL by aspiration with a water pump and attached Pasteur pipette. After suspension through scraping (Sarstedt), the cells were added to the second bottle, from which the complete medium was aspirated. The collection of suspended cells from the two bottles was transferred to a 50-mL Falcon tube and centrifuged for 6 min at 1,500*g*. The supernatant was poured off, and the tube containing the pellet was frozen in liquid nitrogen and stored at −80°C until RNA preparation.

cDNA-AFLP-Based Transcript Profiling

Total RNA was extracted from each cell sample using the RNeasy Plant Mini Kit (Qiagen). Cell lysis was achieved by mechanical disruption in 600 μL of RNeasy Lysis buffer (Qiagen) by highest speed agitation with glass/zirconium beads (0.1 mm diameter; Biospec) on a bead mill (Retsch). All other steps for RNA extraction were done according to the manufacturer's instructions. RNA concentration and purity were assessed by spectrophotometry (Nanodrop ND-1000 spectrophotometer) and denaturing agarose gel electro-

phoresis. First- and second-strand cDNA synthesis and cDNA-AFLP analysis, with *Bst*YI and *Mse*I as restriction enzymes, were carried out according to Vuylsteke et al. (2007), starting from 2 μg of total RNA. The final selection of the cDNA-AFLP amplification products was done with three selective nucleotides, resulting in 128 primer combinations. Expression profiles across the 13 time points for each genotype were quantified with AFLP-Quantar*Pro* software (Keygene). The raw expression values within each genotype were normalized per gene by subtracting the average expression value of each gene from each data point in the time series and dividing it by the SD. Reproducibility of expression profiles between strains F_1-8B and F_1-9A was estimated for every gene by calculating a Pearson correlation between normalized expression data. Expression profiles showing a positive and significant ($P <$ 0.05) correlation across the two strains were submitted to adaptive quality-based clustering (De Smet et al., 2002). The minimal number of genes in a cluster was set to 10, and the minimal probability of genes belonging to a cluster was set to 0.95. Hierarchical clustering (Eisen et al., 1998) was performed with TMEV software (Saeed et al., 2003).

Identification of Differentially Expressed Genes

TDFs were purified from the gel, followed by amplification and subsequent sequencing as described by Vuylsteke et al. (2007). The sequence quality was checked through inspection of the electrophoretic peaks. With the good-quality sequences, a similarity search was done with BLASTN and BLASTX sequence alignments (Altschul et al., 1997) against nucleotide and protein sequences in the publicly available GenBank databases, to which the latest versions of the more recently released genomes of *Phytophthora soja* (U.S. Department of Energy Joint Genome Institute [JGI], v1.1), *Phytophthora ramorum* (JGI, v1.1), *Phaeodactylum tricornutum* (JGI, v2.0), and *Thalassiosira pseudonana* (JGI, v3.0) were added. In case a BLASTN alignment of more than 30 nucleotides with 80% coverage between the query and the hit alignment was achieved, the hit sequence was used as a query for similarity searching with BLASTX. Based on the homology (E-value cutoff, 1×10^{-3}; lowest percentage identification, 29) and the identity of functional GO domains and InterPro domains, the TDFs were functionally annotated and classified into 11 functional groups. TDFs without functional annotation were classified as unknown. GO and InterPro annotations were performed with the online version of the Blast2GO v1.7.2 program (www.Blast2GO.de; Conesa et al., 2005). The program extracts the GO terms associated with homologies identified with the National Center for Biotechnology Information's QBLAST and returns a list of GO annotations represented as hierarchical categories of increasing specificity. Because the diatom genome sequences are not included yet in GenBank, we used the complete sequences of their corresponding diatom genes as input sequences. For the construction of Supplemental Figure S10, the data were analyzed at level 2 and GO classes were set to represent at least five different TDFs.

Cloning of Putative FtsZ cDNA from *S. robusta*

Based on conserved amino acid regions of known *FtsZ* genes in *P. tricornutum* (JGI, v2.0 protein identifiers 14995 and 14426) and *T. pseudonana* (JGI, v3.0 protein identifiers 35728, 269655, and 15398), 12 oligonucleotide primers were designed with CODEHOP (CDH; Rose et al., 1998) and by manual (m) design (Supplemental Fig. S5). These primers were tested in pairwise combinations, and three (m_FP1, m_RP1b, and CDH_FP4) were successfully used to amplify FtsZ cDNA. First, PCR with m_FP1 and m_RP1b primers corresponding to amino acid sequences W(A/S)(I/L/V)NTDAQA and (I/V)NVDFAD, respectively, was carried out using hot-start PCR (AmpliTaq Gold DNA polymerase; Applied Biosystems) in five steps: 9 min at 95°C; four cycles of 1 min at 94°C, 1 min at 35°C, and 1 min at 72°C; four cycles of 1 min at 94°C, 1 min at 45°C, and 1 min at 72°C; 30 cycles of 1 min at 94°C, 1 min at 50°C, and 1 min at 72°C; and one cycle of 10 min at 72°C. A 20-fold-diluted, pooled cDNA sample constituting all cell cycle phases during synchronization was used as template, and 20 pmol of each primer was used in the 25-μL reaction mixture. The PCR products were analyzed on a 1.5% agarose gel, and a band of the correct size (approximately 500 bp) was isolated from the gel and extracted with Nucleospin Extract II (Macherey-Nagel). This extract served as a template in the subsequent PCR with nested primer CDH_FP4, corresponding to amino acid sequence VGIVTKPF, and primer m_RP1b under the following conditions: 9 min at 95°C; 35 cycles of 45 s at 94°C, 1 min at 52°C, and 1 min at 72°C; followed by one cycle of 10 min at 72°C. The resulting DNA fragment of correct size (approximately 300 bp) was ligated into a pCR 4 TOPO vector (Invitrogen) and sequenced. The DNA

sequence of the insert was 92% identical to that of the *P. tricornutum* FtsZ protein 14995. Two specific primers (Sr FtsZ-FP and Sr FtsZ-RP) were designed with Roche ProbeFinder on the cloned sequence for RT-Q-PCR.

RT-Q-PCR Assay

RNA was isolated and quantified as before. Isolated RNA was treated with DNaseI (GE-Healthcare) to remove all contaminating genomic DNA. An aliquot of 0.5 μg of total RNA from each sample was used for cDNA synthesis. The reverse transcription was carried out in a total volume of 20 μL with oligo(dT) primers and the SuperScript II kit (Invitrogen) according to the manufacturer's instructions. A 0.5-μL aliquot of a 5-fold dilution of the cDNA (2.5 ng) served as template for each RT-Q-PCR. Primers for *FCP* quantification and normalization were designed using the Beacon Designer 7.0 (Premier Biosoft International; Supplemental Fig. S5) together with a stringent set of primer design criteria, including predicted melting temperatures of 58.0°C ± 2.0°C, primer lengths of 17 to 22 nucleotides, and amplicon lengths of 75 to 150 bp. Primer pairs were tested by RT-Q-PCR on a pooled cDNA sample under the same conditions as described below. Primer reliability was confirmed by the appearance of a single peak in the melting curve analysis performed by the PCR machine after completion of the amplification reaction.

Eight constitutively and moderately expressed cDNA-AFLP TDFs were selected as candidate genes to serve for internal reference during RT-Q-PCR. These TDFs were excised from the cDNA-AFLP gels, reamplified, and sequenced, and primer pairs were designed as before. The expression stability (M) of the putative normalization genes was analyzed with the geNORM program: genes with the lowest M value are the most stably expressed and were selected as normalization genes (Vandesompele et al., 2002). TDFs sr13af_M281.1 and sr07ae_M536.3 were identified by geNORM to be the two most stably expressed genes (M = 0.426), followed by sr14ah_M385.6 (M = 0.540). The value for the pair-wise variation between two sequential normalization factors (geNORM factor $V_{2/3}$) was 0.146 during synchronization, which is smaller than the cutoff value of 0.15 proposed by Vandesompele et al. (2002) for reliable data normalization. Therefore, all three genes were used for data normalization in the subsequent RT-Q-PCR analyses.

RT-Q-PCR was performed on the Lightcycler 480 (Roche) platform. Each sample was assayed in triplicate under the following conditions: 2.5 ng of template cDNA, 2.5 μL of the Lightcycler 480 SYBR Green I Master Mix (Roche Applied Science), and 2 μL of primers at concentration of 0.5 μM. The cycling conditions comprised 10 min of preincubation at 95°C and 45 cycles of 10 s at 95°C, 15 s at 58°C, and 15 s at 72°C. Amplicon dissociation curves (i.e. melting curves) were recorded by heating at 95°C for 5 s and at 65°C for 1 min. Samples were cooled at 40°C for 10 s. The relative comparison $\Delta\Delta C_t$ method (Pfaffl, 2001) was used to evaluate expression levels of the selected genes relative to the expression of the normalization genes in the same sample. Data were analyzed and normalized with qBase (Hellemans et al., 2007) for expression profile generation.

HPLC Pigment Analysis

S. robusta pigments were sampled from light/dark-synchronized cultures (see above) by filtering 25 mL of suspended culture over a preweighed 25-mm Whatman glass fiber filter. Filters were wrapped in aluminum foil, frozen in liquid nitrogen, and stored at −80°C. Before analysis, the filters were lyophilized for 8 h and weighed (0.1-mg accuracy) to calculate the dry weight of each sample. Pigments were extracted from the filters in 90% acetone by means of sonication (tip sonicator; 40 W for 30 s). Extracts were filtered over a 0.2-μm Alltech nylon syringe filter to remove particles and injected into a Agilent 1100 series HPLC system (ChemStation software) equipped with a Macherey-Nagel reverse-phase C18 column (Nucleodur C18 pyramid; 5 μm particle size). Pigments were analyzed according to the method of Wright and Jeffrey (1997) using a gradient of three solvents: 80% methanol-20% ammonium acetate, 90% acetonitrile, and ethyl acetate. Two detectors were connected to the HPLC system: an Agilent standard fluorescence detector to measure fluorescence of chlorophylls and their derivatives and an Agilent diode array detector to measure absorbance of each peak at 436 and 665 nm and absorbance spectra over a 400- to 700-nm range. Fucoxanthin was identified by comparison of retention times and absorbance spectra and quantified by calculating response factors using pure pigment standards (supplied by DHI).

Sequence data from this article can be found in the GenBank/EMBL data libraries under accession numbers FJ388875 and GE343005 to GE343326.

Supplemental Data

The following material is available in the online version of this article.

Supplemental Figure S1. Schematic presentation of the chloroplastidic events during the cell cycle of *S. robusta*.

Supplemental Figure S2. Flow cytometric DNA content histograms for assessing the S-phase cell cycle arrest by HU.

Supplemental Figure S3. Estimation method for percentage of cells in different cell cycle phases based on photographs of the synchronized culture.

Supplemental Figure S4. Laser-scanning confocal photographs of a *S. robusta* cell to illustrate the addition of one girdle band.

Supplemental Figure S5. Identification of a *S. robusta* FtsZ ortholog and design of specific RT-Q-PCR primers for *FtsZ* and *FCP* quantification.

Supplemental Figure S6. Section of an electropherogram of the cDNA-AFLP fingerprint of the two *S. robusta* strains.

Supplemental Figure S7. The nine clusters identified by adaptive quality-based clustering (De Smet et al., 2002) of 917 expression profiles that were highly reproducible.

Supplemental Figure S8. Expression of the *S. robusta* MCM5 and histone H3 ortholog as a function of time after reillumination.

Supplemental Figure S9. Clustering of the expression profiles of the cell cycle-modulated, annotated TDFs.

Supplemental Figure S10. Blast2GO pie chart representing the distribution of functional GO labels for biological processes.

Supplemental Figure S11. Expression of the *S. robusta* orthologs of β-tubulin and the WD40-repeat protein as a function of time after reillumination.

Supplemental Table S1. Representation of the cDNA-AFLP analysis, including all quantified TDFs, annotations, and expression data.

Supplemental Table S2. Distribution of selected genes with respect to their expression cluster.

Supplemental Table S3. Mapping of GO labels to the annotated TDFs, together with their assigned functional categories.

Supplemental Table S4. Mapping of InterPro domains to the annotated TDFs.

Supplemental Table S5. Calculation of χ^2 correlation between photosynthetic genes and expression cluster C7-L.

ACKNOWLEDGMENTS

LITERATURE CITED

Adams S, Maple J, Moller SG (2008) Functional conservation of the MIN plastid division homologues of *Chlamydomonas reinhardtii*. Planta 227: 1199–1211

Altschul SF, Madden TL, Schäffer AA, Zhang J, Zhang Z, Miller W, Lipman DJ (1997) Gapped BLAST and PSI-BLAST: a new generation of protein database search programs. Nucleic Acids Res 25: 3389–3402

Apel K, Hirt H (2004) Reactive oxygen species: metabolism, oxidative stress, and signal transduction. Annu Rev Plant Biol 55: 373–399

Apt KE, Zaslavkaia L, Lippmeier JC, Lang M, Kilian O, Wetherbee R, Grossman AR, Kroth PG (2002) In vivo characterization of diatom multipartite plastid targeting signals. J Cell Sci 115: 4061–4069

Armbrust EV, Berges JA, Bowler C, Green BR, Martinez D, Putnam NH, Zhou S, Allen AE, Apt KE, Bechner M, et al (2004) The genome of the diatom *Thalassiosira pseudonana*: ecology, evolution, and metabolism. Science 306: 79–86

Banse K (1982) Cell volumes, maximal growth rates of unicellular algae and ciliates, and the role of ciliates in the marine pelagial. Limnol Oceanogr 27: 1059–1071

Beech PL, Gilson PR (2000) FtsZ and organelle division in protists. Protist 151: 11–16

Bhaya D, Grossman AR (1993) Characterization of gene clusters encoding the fucoxanthin chlorophyll proteins of the diatom *Phaeodactylum tricornutum*. Nucleic Acids Res 21: 4458–4466

Bowler C, Allen AE, Badger JH, Grimwood J, Jabbari K, Kuo A, Maheswari U, Martens C, Maumus F, Otillar RP, et al (2008) The *Phaeodactylum* genome reveals the dynamic nature and multi-lineage evolutionary history of diatom genomes. Nature (in press)

Breyne P, Dreesen R, Vandepoele K, De Veylder L, Van Breusegem F, Callewaert L, Rombauts S, Raes J, Cannoot B, Engler G, et al (2002) Transcriptome analysis during cell division in plants. Proc Natl Acad Sci USA 99: 14825–14830

Brzezinski MA, Olson RJ, Chisholm SW (1990) Silicon availability and cell-cycle progression in marine diatoms. Mar Ecol Prog Ser 67: 83–96

Butko P, Szalay L (1985) Photosystem II and its connection to the electron transport chain during the life cycle of *Chlorella*. Photobiochem Photobiophys 10: 93–103

Chan AT (1978) Comparative physiological study of marine diatoms and dinoflagellates in relation to irradiance and cell size. I. Growth under continuous light. J Phycol 14: 396–402

Chan AT (1980) Comparative physiological study of marine diatoms and dinoflagellates in relation to irradiance and cell size. II. Relationship between photosynthesis, growth, and carbon/chlorophyll *a* ratio. J Phycol 16: 428–432

Chepurnov VA, Mann DG, von Dassow P, Vanormelingen P, Gillard J, Inzé D, Sabbe K, Vyverman W (2008) In search of new tractable diatoms for experimental biology. Bioessays 30: 692–702

Chepurnov VA, Mann DG, Vyverman W, Sabbe K, Danielidis DB (2002) Sexual reproduction, mating system, and protoplast dynamics of *Seminavis* (Bacillariophyceae). J Phycol 38: 1004–1019

Chiappino ML, Volcani BE (1977) Studies on biochemistry and fine structure of silica shell formation in diatoms. VII. Sequential cell wall development in the pennate *Navicula pelliculosa*. Protoplasma 93: 205–221

Chiovitti A, Ngoh JE, Wetherbee R (2006) 1,3-Beta-D-glucans from *Haramonas dimorpha* (Raphidophyceae). Bot Mar 49: 360–362

Cho RJ, Huang M, Campbell MJ, Dong H, Steinmetz L, Sapinoso L, Hampton G, Elledge SJ, Davis RW, Lockhart DJ (2001) Transcriptional regulation and function during the human cell cycle. Nat Genet 27: 48–54

Claquin P, Kromkamp JC, Martin-Jezequel V (2004) Relationship between photosynthetic metabolism and cell cycle in a synchronized culture of the marine alga *Cylindrotheca fusiformis* (Bacillariophyceae). Eur J Phycol 39: 33–41

Cohn SA, Disparti NC (1992) Analysis of environmental influences on diatom cell motility. Mol Biol Cell 3: A361

Coleman AW, Nerozzi AM (1999) Temporal and spatial coordination of cells with their plastid component. Int Rev Cytol 193: 125–164

Conesa A, Götz S, García-Gómez JM, Terol J, Talón M, Robles M (2005) Blast2GO: a universal tool for annotation, visualization and analysis in functional genomics research. Bioinformatics 21: 3674–3676

Coombs J, Darley WM, Holm-Hansen O, Volcani BE (1967a) Studies on the biochemistry and fine structure of silica shell formation in diatoms: chemical composition of *Navicula pelliculosa* during silicon-starvation synchrony. Plant Physiol 42: 1601–1606

Coombs J, Halicki PJ, Holm-Hansen O, Volcani BE (1967b) Studies on the biochemistry and fine structure of silica shell formation in diatoms: changes in concentration of nucleoside triphosphates during synchronized division of *Cylindrotheca fusiformis* Reimann and Lewin. Exp Cell Res 47: 302–314

Danielidis DB, Mann DG (2002) The systematics of *Seminavis* (Bacillariophyta): the lost identities of *Amphora angusta*, *A. ventricosa* and *A. macilenta*. Eur J Phycol 37: 429–448

Dawson PA (1973) Observations on the structure of some forms of *Gomphonema parvulum* Kütz. III. The internal organization. J Phycol 9: 165–175

de Francisco A, Roth LE (1977) Marine diatom, *Striatella unipunctata*. I. Cytoplasmic fine structure with emphasis on Golgi apparatus. Cytobiologie 14: 191–206

De Smet F, Mathys J, Marchal K, Thijs G, De Moor B, Moreau Y (2002) Adaptive quality-based clustering of gene expression profiles. Bioinformatics 18: 735–746

De Veylder L, Beeckman T, Inzé D (2007) The ins and outs of the plant cell cycle. Nat Rev Mol Cell Biol 8: 655–665

Diwu Z, Chen C-S, Zhang C, Klaubert DH, Haugland RP (1999) A novel acidotropic pH indicator and its potential application in labeling acidic organelles of live cells. Chem Biol 6: 411–418

Durnford DG, Falkowski PG (1997) Chloroplast redox regulation of nuclear gene transcription during photoacclimation. Photosynth Res 53: 229–241

Eisen MB, Spellman PT, Brown PO, Botstein D (1998) Cluster analysis and display of genome-wide expression patterns. Proc Natl Acad Sci USA 95: 14863–14868; erratum Eisen MB, Spellman PT, Brown PO, Botstein D (1998) Proc Natl Acad Sci USA 96: 10943

El-Shami M, El-Kafafi S, Falconet D, Lerbs-Mache S (2002) Cell cycle-dependent modulation of FtsZ expression in synchronized tobacco BY2 cells. Mol Genet Genomics 267: 254–261

Eppard M, Rhiel E (1998) The genes encoding light-harvesting subunits of Cyclotella cryptica (Bacillariophyceae) constitute a complex and heterogeneous family. Mol Gen Genet 260: 335–345

Eppard M, Rhiel E (2000) Investigations on gene copy number, introns and chromosomal arrangement of genes encoding the fucoxanthin chlorophyll a/c-binding proteins of the centric diatom Cyclotella cryptica. Protist 151: 27–39

Falkowski PG, Dubinsky Z, Wyman K (1985) Growth-irradiance relationships in phytoplankton. Limnol Oceanogr 30: 311–321

Falkowski PG, Katz ME, Knoll AH, Quigg A, Raven JA, Schofield O, Taylor FJR (2004) The evolution of modern eukaryotic phytoplankton. Science 305: 354–360

Falkowski PG, LaRoche J (1991) Acclimation to spectral irradiance in algae. J Phycol 27: 8–14

Fernie AR, Carrari F, Sweetlove LJ (2004) Respiratory metabolism: glycolysis, the TCA cycle and mitochondrial electron transport. Curr Opin Plant Biol 7: 254–261

Frigeri LG, Radabaugh TR, Haynes PA, Hildebrand M (2006) Identification of proteins from a cell wall fraction of the diatom Thalassiosira pseudonana: insights into silica structure formation. Mol Cell Proteomics 5: 182–193

Furusato E, Asaeda T, Manatunge J (2004) Tolerance for prolonged darkness of three phytoplankton species, Microcystis aeruginosa (Cyanophyceae), Scenedesmus quadricauda (Chlorophyceae), and Melosira ambigua (Bacillariophyceae). Hydrobiologia 527: 153–162

Gee RW, Byerrum RU, Gerber DW, Tolbert NE (1988) Dihydroxyacetone phosphate reductase in plants. Plant Physiol 86: 98–103

Goericke R, Welschmeyer NA (1992) Pigment turnover in the marine diatom Thalassiosira weissflogii. 2. The $^{14}CO_2$-labeling kinetics of carotenoids. J Phycol 28: 507–517

Granum E, Raven JA, Leegood RC (2005) How do marine diatoms fix 10 billion tonnes of inorganic carbon per year? Can J Bot 83: 898–908

Green BR, Durnford DG (1996) The chlorophyll-carotenoid proteins of oxygenic photosynthesis. Annu Rev Plant Physiol Plant Mol Biol 47: 685–714

Guglielmi G, Lavaud J, Rousseau B, Etienne A-L, Houmard J, Ruban AV (2005) The light-harvesting antenna of the diatom Phaeodactylum tricornutum: evidence for a diadinoxanthin-binding subcomplex. FEBS J 272: 4339–4348

Guillard RRL (1975) Culture of Phytoplankton for Feeding Marine Invertebrates. Plenum Press, New York

Hashimoto H (2005) The ultrastructural features and division of secondary plastids. J Plant Res 118: 163–172

Haswell ES, Meyerowitz EM (2006) MscS-like proteins control plastid size and shape in Arabidopsis thaliana. Curr Biol 16: 1–11

Hazelaar S, van der Strate HJ, Gieskes WWC, Vrieling EG (2005) Monitoring rapid valve formation in the pennate diatom Navicula salinarum (Bacillariophyceae). J Phycol 41: 354–358

Hellemans J, Mortier G, De Paepe A, Speleman F, Vandesompele J (2007) qBase relative quantification framework and software for management and automated analysis of real-time quantitative PCR data. Genome Biol 8: R19

Hildebrand M, Frigeri LG, Davis AK (2007) Synchronized growth of Thalassiosira pseudonana (Bacillariophyceae) provides novel insights into cell-wall synthesis processes in relation to the cell cycle. J Phycol 43: 730–740

Hoagland KD, Rosowski JR, Gretz MR, Roemer SC (1993) Diatom extracellular polymeric substances: function, fine-structure, chemistry, and physiology. J Phycol 29: 537–566

Horton P, Ruban AV, Walters RG (1996) Regulation of light harvesting in green plants. Annu Rev Plant Physiol Plant Mol Biol 47: 655–684

Hu Y, Chen ZW, Liu WZ, Liu XL, He YK (2008) Chloroplast division is regulated by the circadian expression of FTSZ and MIN genes in Chlamydomonas reinhardtii. Eur J Phycol 43: 207–215

Iida R, Yasuda T, Tsubota E, Takatsuka H, Masuyama M, Matsuki T, Kishi K (2003) M-LP, Mpv17-like protein has a peroxisomal membrane targeting signal comprising a transmembrane domain and a positively charged loop and up-regulates expression of the manganese superoxide dismutase gene. J Biol Chem 278: 6301–6306

Ikegami S, Taguchi T, Ohashi M, Oguro M, Nagano H, Mano Y (1978) Aphidicolin prevents mitotic cell division by interfering with the activity of DNA polymerase-α. Nature 275: 458–460

Itoh R, Takahashi H, Toda K, Kuroiwa H, Kuroiwa T (1996) Aphidicolin uncouples the chloroplast division cycle from the mitotic cycle in the unicellular red alga Cyanidioschyzon merolae. Eur J Cell Biol 71: 303–310

Johanningmeier U, Howell SH (1984) Regulation of light-harvesting chlorophyll-binding protein messenger-RNA accumulation in Chlamydomonas reinhardtii: possible involvement of chlorophyll synthesis precursors. J Biol Chem 259: 3541–3549

Kaftan D, Meszaros T, Whitmarsh J, Nedbal L (1999) Characterization of photosystem II activity and heterogeneity during the cell cycle of the green alga Scenedesmus quadricauda. Plant Physiol 120: 433–441

Kapros T, Bögre L, Németh K, Bakó L, Györgyey J, Wu SC, Dudits D (1992) Differential expression of histone H3 gene variants during cell cycle and somatic embryogenesis in alfalfa. Plant Physiol 98: 621–625

Kiefel BR, Gilson PR, Beech PL (2004) Diverse eukaryotes have retained mitochondrial homologues of the bacterial division protein FtsZ. Protist 155: 105–115

Kilian O, Kroth PG (2005) Identification and characterization of a new conserved motif within the presequence of proteins targeted into complex diatom plastids. Plant J 41: 175–183

Kooistra WH, De Stefano M, Mann DG, Medlin LK (2003) The phylogeny of diatoms. In WEG Müller, ed, Silicon Biomineralization: Progress in Molecular and Subcellular Biology, Vol 33. Springer-Verlag, New York, pp 59–97

Koussevitzky S, Nott A, Mockler TC, Hong F, Sachetto-Martins G, Surpin M, Lim IJ, Mittler R, Chory J (2007) Signals from chloroplasts converge to regulate nuclear gene expression. Science 316: 715–719

Kröger N, Wetherbee R (2000) Pleuralins are involved in theca differentiation in the diatom Cylindrotheca fusiformis. Protist 151: 263–73

Krupinska K, Humbeck K (1994) Light-induced synchronous cultures, an excellent tool to study the cell cycle of unicellular green algae. J Photochem Photobiol B Biol 26: 217–231

Krzeszowiec W, Rajwa B, Dobrucki J, Gabrys H (2007) Actin cytoskeleton in Arabidopsis thaliana under blue and red light. Biol Cell 99: 251–260

Lavaud J, Rousseau B, Etienne A-L (2004) General features of photoprotection by energy dissipation in planktonic diatoms (Bacillariophyceae). J Phycol 40: 130–137

Leblanc C, Falciatore A, Watanabe M, Bowler C (1999) Semi-quantitative RT-PCR analysis of photoregulated gene expression in marine diatoms. Plant Mol Biol 40: 1031–1044

Leblanc K, Hutchins DA (2005) New applications of a biogenic silica deposition fluorophore in the study of oceanic diatoms. Limnol Oceanogr Methods 3: 462–476

Lee M, Li C-W (1992) The origin of the silica deposition vesicle of diatoms. Bot Bull Acad Sin 33: 317–325

Maeshima M (2001) Tonoplast transporters: organization and function. Annu Rev Plant Physiol Plant Mol Biol 52: 469–497

Mann DG (1996) Chloroplast morphology, movements and inheritance in diatoms. In BR Chaudhary, SB Agrawal, eds, Cytology, Genetics and Molecular Biology of Algae. SPB Academic Publishing, Amsterdam, pp 249–274

Margolin W (2005) FtsZ and the division of prokaryotic cells and organelles. Nat Rev Mol Cell Biol 6: 862–871

Mayama S, Kuriyama A (2002) Diversity of mineral cell coverings and their formation processes: a review focused on the siliceous cell coverings. J Plant Res 115: 289–295

McFadden GI (2001) Chloroplast origin and integration. Plant Physiol **125**: 50–53

Menges M, Hennig L, Gruissem W, Murray JAH (2002) Cell cycle-regulated gene expression in *Arabidopsis*. J Biol Chem **277**: 41987–42002

Mereschkowsky C (1904) Loi de translation des stades chez les diatomées. J Bot **18**: 17–29, 76–83

Montsant A, Allen AE, Coesel S, De Martino A, Falciatore A, Mangogna M, Siaut M, Heijde M, Jabbari K, Maheswari U, et al (2007) Identification and comparative genomic analysis of signaling and regulatory components in the diatom *Thalassiosira pseudonana*. J Phycol **43**: 585–604

Nishida K, Yagisawa F, Kuroiwa H, Nagata T, Kuroiwa T (2005) Cell cycle-regulated, microtubule-independent organelle division in *Cyanidioschyzon merolae*. Mol Biol Cell **16**: 2493–2502

Nott A, Jung HS, Koussevitzky S, Chory J (2006) Plastid-to-nucleus retrograde signaling. Annu Rev Plant Biol **57**: 739–759

Oeltjen A, Krumbein WE, Rhiel E (2002) Investigations on transcript sizes, steady state mRNA concentrations and diurnal expression of genes encoding fucoxanthin chlorophyll *a/c* light harvesting polypeptides in the centric diatom *Cyclotella cryptica*. Plant Biol **4**: 250–257

Oeltjen A, Marquardt J, Rhiel E (2004) Differential circadian expression of genes *fcp2* and *fcp6* in *Cyclotella cryptica*. Int Microbiol **7**: 127–131

Ohlrogge J, Browse J (1995) Lipid biosynthesis. Plant Cell **7**: 957–970

Olson RJ, Vaulot D, Chisholm SW (1986) Effects of environmental stresses on the cell cycle of two marine phytoplankton species. Plant Physiol **80**: 918–925

Osteryoung KW, Nunnari J (2003) The division of endosymbiotic organelles. Science **302**: 1698–1704

Osteryoung KW, Vierling E (1995) Conserved cell and organelle division. Nature **376**: 473–474

Otero A, Goto K (2005) Microalgae: the 'self-synchronized' eukaryotes. Trends Biotechnol **23**: 448–449

Pfaffl MW (2001) A new mathematical model for relative quantification in real-time RT-PCR. Nucleic Acids Res **29**: e45

Pickett-Heaps J, Schmid AMM, Edgar LA (1990) The cell biology of diatom valve formation. *In* FE Round, DJ Chapman, eds, Progress in Phycological Research, Vol 7. Biopress, Bristol, UK, pp 1–168

Pirson A, Lorenzen H (1966) Synchronized dividing algae. Annu Rev Plant Physiol **17**: 439-458

Post AF, Eijgenraam F, Mur LR (1985) Influence of light period length on photosynthesis and synchronous growth of the green alga *Scenedesmus protuberans*. Br Phycol J **20**: 391–397

Pyke KA (1999) Plastid division and development. Plant Cell **11**: 549–556

Ragni M, Ribera d'Alcalà M (2007) Circadian variability in the photobiology of *Phaeodactylum tricornutum*: pigment content. J Plankton Res **29**: 141–156

Raven JA, Geider RJ (1988) Temperature and algal growth. New Phytol **110**: 441–461

Raynaud C, Perennes C, Reuzeau C, Catrice O, Brown S, Bergounioux C (2005) Cell and plastid division are coordinated through the prereplication factor AtCDT1. Proc Natl Acad Sci USA **102**: 8216–8221

Riebesell U (2000) Carbon fix for a diatom. Nature **407**: 959–960

Riper DM, Owens TG, Falkowski PG (1979) Chlorophyll turnover in *Skeletonema costatum*, a marine plankton diatom. Plant Physiol **64**: 49–54

Roberts K, Granum E, Leegood RC, Raven JA (2007) Carbon acquisition by diatoms. Photosynth Res **93**: 79–88

Rose TM, Schultz ER, Henikoff JG, Pietrokovskin S, McCallum CM, Henikoff S (1998) Consensus-degenerate hybrid oligonucleotide primers for amplification of distantly-related sequences. Nucleic Acids Res **26**: 1628–1635

Ruban AV, Lavaud J, Rousseau B, Guglielmi G, Horton P, Etienne A-L (2004) The super-excess energy dissipation in diatom algae: comparative analysis with higher plants. Photosynth Res **82**: 165–175

Saeed AI, Sharov V, White J, Li J, Liang W, Bhagabati N, Braisted J, Klapa M, Currier T, Thiagarajan M, et al (2003) TM4: a free, open-source system for microarray data management and analysis. Biotechniques **34**: 374–378

Sarthou G, Timmermans KR, Blain S, Tréguer P (2005) Growth physiology and fate of diatoms in the ocean: a review. J Sea Res **53**: 25–42

Setlikova E, Setlik I, Kupper H, Kasalicky V, Prasil O (2005) The photosynthesis of individual algal cells during the cell cycle of Scenedesmus quadricauda studied by chlorophyll fluorescence kinetic microscopy. Photosynth Res **84**: 113–120

Shimizu K, Del Amo Y, Brzezinski MA, Stucky GD, Morse DE (2001) A novel fluorescent silica tracer for biological silicification studies. Chem Biol **8**: 1051–1060

Siaut M, Heijde M, Mangogna M, Montsant A, Coesel S, Allen A, Manfredonia A, Falciatore A, Bowler C (2007) Molecular toolbox for studying diatom biology in *Phaeodactylum tricornutum*. Gene **406**: 23–35

Sipiczki M (2007) Splitting of the fission yeast septum. FEMS Yeast Res **7**: 761–770

Stoermer EF, Pankratz HS, Bowen CC (1965) Fine structure of the diatom *Amphipleura pellucida*. II. Cytoplasmic fine structure and frustule formation. Am J Bot **52**: 1067–1078

Takahara M, Takahashi H, Matsunaga S, Miyagishima S, Takano H, Sakai A, Kawano S, Kuroiwa T (2000) A putative mitochondrial FtsZ gene is present in the unicellular primitive red alga *Cyanidioschyzon merolae*. Mol Gen Genet **264**: 452–460

Takisawa H, Mimura S, Kubota Y (2000) Eukaryotic DNA replication: from pre-replication complex to initiation complex. Curr Opin Cell Biol **12**: 690–696

Tamiya H (1966) Synchronous cultures of algae. Annu Rev Plant Physiol **17**: 1-26

Tang EPY (1996) Why do dinoflagellates have lower growth rates? J Phycol **32**: 80–84

Thompson SEM, Taylor AR, Brownlee C, Callow ME, Callow JA (2008) The role of nitric oxide in diatom adhesion in relation to substratum properties. J Phycol **44**: 967–976

Tsuruga H, Yabuta N, Hashizume K, Ikeda M, Endo Y, Nojima H (1997) Expression, nuclear localization and interactions of human MCM/P1 proteins. Biochem Biophys Res Commun **236**: 118–125

Tukaj Z, Matusiak-Mikulin K, Lewandowska J, Szurkowski J (2003) Changes in the pigment patterns and the photosynthetic activity during a light-induced cell cycle of the green alga *Scenedesmus armatus*. Plant Physiol Biochem **41**: 337–344

Vandesompele J, De Preter K, Pattyn F, Poppe B, Van Roy N, De Paepe A, Speleman F (2002) Accurate normalization of real-time quantitative RT-PCR data by geometric averaging of multiple internal control genes. Genome Biol **3**: research0034.1–research0034.11

Vaulot D, Olson RJ, Chisholm SW (1986) Light and dark control of the cell cycle in two marine phytoplankton species. Exp Cell Res **167**: 38–52

von Wettstein D, Gough S, Kannangara CG (1995) Chlorophyll biosynthesis. Plant Cell **7**: 1039–1057

Vuylsteke M, Peleman JD, van Eijk MJT (2007) AFLP-based transcript profiling (cDNA-AFLP) for genome-wide expression analysis. Nat Protocols **2**: 1399–1413

Vuylsteke M, Van Den Daele H, Vercauteren A, Zabeau M, Kuiper M (2006) Genetic dissection of transcriptional regulation by cDNA-AFLP. Plant J **45**: 439–446

Weart RB, Nakano S, Lane BE, Zuber P, Levin PA (2005) The ClpX chaperone modulates assembly of the tubulin-like protein FtsZ. Mol Microbiol **57**: 238–249

Wetherbee R, Lind JL, Burke J, Quatrano RS (1998) The first kiss: establishment and control of initial adhesion by raphid diatoms. J Phycol **34**: 9–15

Wilhelm C, Büchel C, Fisahn J, Goss R, Jakob T, LaRoche J, Lavaud J, Lohr M, Riebesell U, Stehfest K, et al (2006) The regulation of carbon and nutrient assimilation in diatoms is significantly different from green algae. Protist **157**: 91–124

Winter J, Brandt P (1986) Stage-specific state I-state II transitions during the cell cycle of *Euglena gracilis*. Plant Physiol **81**: 548–552

Wolfe-Simon F, Starovoytov V, Reinfelder JR, Schofield O, Falkowski PG (2006) Localization and role of manganese superoxide dismutase in a marine diatom. Plant Physiol **142**: 1701–1709

Wright SW, Jeffrey SW (1997) High resolution system for chlorophylls and carotenoids of marine phytoplankton. *In* SW Jeffrey, RFC Mantoura, SW Wright, eds, Phytoplankton Pigments in Oceanography: A Guide to Advanced Methods. SCOR-UNESCO, Paris, pp 327–341

Yeong FM (2005) Severing all ties between mother and daughter: cell separation in budding yeast. Mol Microbiol **55**: 1325–1331

Young CW, Hodas S (1964) Hydroxyurea: inhibitory effect on DNA metabolism. Science **146**: 1172–1174

Zurzolo C, Bowler C (2001) Exploring bioinorganic pattern formation in diatoms: a story of polarized trafficking. Plant Physiol **127**: 1339–1345